Rail. Eng. Science (2020) 28(2):160–183
https://doi.org/10.1007/s40534-020-00212-z

Rotary-scaling fine-tuning (RSFT) method for optimizing railway wheel profiles and its application to a locomotive

Yunguang Ye[1] · Yayun Qi[2] · Dachuan Shi[1] · Yu Sun[2,3] · Yichang Zhou[1] · Markus Hecht[1]

Received: 13 April 2020 / Revised: 4 May 2020 / Accepted: 11 May 2020 / Published online: 16 June 2020

Abstract The existing multi-objective wheel profile optimization methods mainly consist of three sub-modules: (1) wheel profile generation, (2) multi-body dynamics simulation, and (3) an optimization algorithm. For the first module, a comparably conservative rotary-scaling fine-tuning (RSFT) method, which introduces two design variables and an empirical formula, is proposed to fine-tune the traditional wheel profiles for improving their engineering applicability. For the second module, for the TRAXX locomotives serving on the Blankenburg–Rübeland line, an optimization function representing the relationship between the wheel profile and the wheel–rail wear number is established based on Kriging surrogate model (KSM). For the third module, a method combining the regression capability of KSM with the iterative computing power of particle swarm optimization (PSO) is proposed to quickly and reliably implement the task of optimizing wheel profiles. Finally, with the RSFT–KSM–PSO method, we propose two wear-resistant wheel profiles for the TRAXX locomotives serving on the Blankenburg–Rübeland line, namely S1002-S and S1002-M. The S1002-S profile minimizes the total wear number by 30%, while the S1002-M profile makes the wear distribution more uniform through a proper sacrifice of the tread wear number, and the total wear number is reduced by 21%. The quasi-static and hunting stability tests further demonstrate that the profile designed by the RSFT–KSM–PSO method is promising for practical engineering applications.

Keywords Wheel profile optimization · Wear reduction · Rotary-scaling fine-tuning · Particle swarm optimization · Kriging surrogate model

1 Introduction

Reducing wheel wear has been a topic of concern since railway vehicles emerge. Most directly, slow wheel wear can improve wheel-track system performances, extend wheel re-profiling mileage, and reduce maintenance costs [1–3]. At present, the works on wheel wear reduction are mainly based on five aspects: (1) wheel–rail tribology [4–8], (2) wheel/rail profile optimization [9], (3) vehicle/track design [10–13], (4) active control of vehicle suspensions [14–17], and (5) track layout setting [18, 19]. This article focuses on wheel profile optimization.

1.1 Existing methods

Since the advent of railway vehicles, the wheel–rail relationship has been a hot topic. The related research is mainly divided into two categories: (1) the wheel–rail contact geometry and (2) the wheel–rail interaction forces and their impact on vehicle-track systems. Both categories of research are based on specific wheel and rail profiles,

✉ Yunguang Ye
yunguang.ye@campus.tu-berlin.de

✉ Yayun Qi
yayun_qi@163.com

[1] Institute of Land and Sea Transport Systems, Technical University of Berlin, 10587 Berlin, Germany

[2] State Key Laboratory of Traction Power, Southwest Jiaotong University, Chengdu 610331, China

[3] College of Transportation Science and Engineering, Nanjing Tech University, Nanjing 210009, China

and therefore, the design and optimization of wheel profiles have always been a topic of interest to scholars. In this section, we briefly review some of the wheel profile optimization methods proposed in the past two decades, which can be used to reduce wheel wear. These methods fall into two groups: single-objective and multi-objective optimization methods.

1.1.1 Single-objective optimization methods

Classical single-objective optimization methods include (I) target contact angle method [20], (II) target RRD (rolling radius difference) method [21–24], (III) target conicity method [25], and (IV) target normal gap method [26], etc.

(I) Target contact angle method Shen et al. [20] proposed a method for designing the wheel profile using the inverse method of contact angle curve and applied it to the profile design of independent wheels and the wheels of low-floor vehicles. In this method, five hypotheses are introduced: (1) the wheel and rail are rigid, (2) the influence of wheelset roll on the contact angle is ignored, (3) the shape of the rail is convex, (4) the shapes of the left and right wheels and rails are symmetrical, and (5) the flange thickness and height, and the wheel width remain unchanged.

In Fig. 1, the wheel and rail profiles are given as $Z_w(Y_w)$ and $Z_r(Y_r)$, respectively. When the wheelset lateral displacement is y_s, the coordinates of the contact point on the wheel and rail are (y_w, z_w) and (y_r, z_r), respectively, where $z_r = Z_r(y_r)$ and $z_w = Z_w(y_w)$. Then, there is

$$Z_w = Z_0 + \int_{y_1}^{y_2} \tan\alpha \, dY_w, \tag{1}$$

where Z_0 is the ordinate of the contact point on the wheel when $y_s = 0$; α is the contact angle, and $\tan\alpha = dZ_w/dY_w = dZ_r/dY_r$. Equation (1) means that the wheel profile can be expressed by $\alpha(Y_w)$.

The shape of the wheel profile designed with this method is not limited to the combination of arcs and straights. However, the effect of the wheelset roll angle is not taken into account in the contact angle.

(II) Target RRD method Shevtsov et al. [21] proposed a method for the optimal design of a wheel profile based on RRD, which was subsequently used in many references.

As plotted in Fig. 2, the curve of the wheel profile is represented by discrete points, where solid points represent fixed points, and hollow points represent movable points. The entire profile is obtained by using a curve fitting method (such as the piecewise cubic Hermite interpolating polynomial [21], and the B-spline [22]) to fit these points. The abscissas $y_i\,(i = 1, 2, \ldots, n)$ of the hollow points are unchanged, but their ordinates $z_i\,(i = 1, 2, \ldots, n)$ are movable, and these ordinates are defined as design variables. Then an objective function [Eq. (2)] is introduced:

$$F_0(x) = \frac{\sum_{i=1}^{k}\left(\Delta r_{y_i}^{\mathrm{tar}}(x) - \Delta r_{y_i}^{\mathrm{calc}}(x)\right)^2}{\sum_{i=1}^{k}\left(\Delta r_{y_i}^{\mathrm{tar}}(x)\right)^2} \to \min, \tag{2}$$

where $\Delta r_{y_i}^{\mathrm{tar}}(x)$ is the target RRD function, $\Delta r_{y_i}^{\mathrm{calc}}(x)$ is the calculated RRD function for the design profile. To ensure the stability of the vehicle and the monotonicity of the tread region of generated wheel profiles, some constraints to limit the equivalent conicity and slope are required (see Ref. [21]).

This method firstly introduces a medium that reflects vehicle dynamics and wheel–rail contact mechanics: the RRD function, through which the optimization of the wheel profile is transformed into the optimization of the RRD function. Due to this transformation, the multi-objective problem of the optimal design of the wheel profile is transformed into a single-objective problem, which reduces the difficulty of solving the optimization problem. The key and difficulty of this method lie in the selection of target RRD function since an appropriate target RRD function is usually based on expertise and repeated attempts. In Ref. [21, 22], three target RRD functions were proposed. A similar method called the target $Y - \Delta r$ method was presented in Ref. [27].

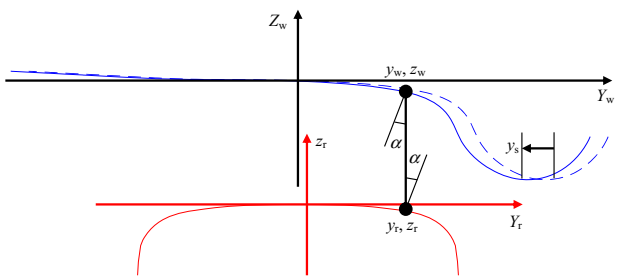

Fig. 1 Sketch of contact points between the wheel and rail

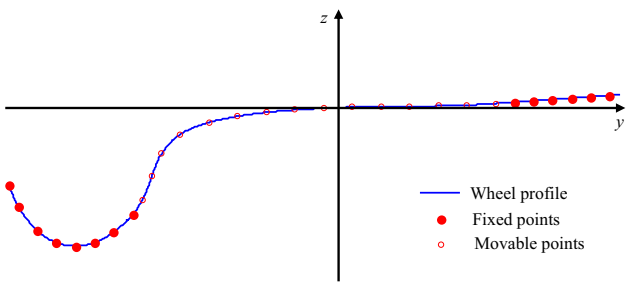

Fig. 2 Fixed and movable points on wheel profile

(III) Target conicity method Polach [25] proposed a method for designing the wheel tread profile to achieve a wide contact spreading and target conicity level, i.e., target conicity method. This method is similar to the target contact angle method [20]. Firstly, five hypotheses are introduced: (1) the wheel and rail are rigid, (2) the wheelset roll angle is ignored, (3) the shape of the rail is convex, (4) the shapes of the left and right wheels and rails are symmetrical, and (5) the contact between wheel and rail is represented by a contact point.

In this method, the design of wheel tread is based on a specified rail profile. As shown in Fig. 1, Y_w and Z_w can be expressed as a function of the wheelset lateral displacement y_s, i.e., $Y_w(s)$ and $Z_w(s)$, respectively. To achieve continuous spreading, lateral distributions of the contact points on the rail profile are assumed proportional to the contact point distribution on the wheel profile. The wheel contact points can be transformed to the contact points on the rail by $Y_r(y_s) = Y_w(y_s) + k_y y_s + Y_0$, where k_y is a coefficient related to RRD and can be used to adjust the target equivalent conicity level and Y_0 is the abscissa of the contact point on the wheel when $y_s = 0$. Then, the wheel profile can be further derived:

$$Z_w = Z_0 + \int_{y_1}^{y_2} Z'_w dY_w, \tag{3}$$

where $Z'_w(Y_w)|y_s = Z'_r(Y_r)|y_s = \tan\alpha$, as plotted in Fig. 3. Finally, the equivalent conicity $\lambda \approx \alpha_0 R_w/(R_w - R_r)$ is proportional to RRD, which can be calculated by subtracting the vertical coordinates of contact points on the left and right wheels $\Delta r(y_s) = (Z_{rL} - Z_{wL}) - (Z_{rR} - Z_{wR})$, where subscripts L and R represent left and right, and α_0 is the contact angle between wheel and rail profiles in the nominal position. The selection of the contact point distribution and the proportionality coefficient k_y is limited by the wheel tread width and the rail width before the flange root contacts the rail gauge corner.

As described in Ref. [25], the application environment of the wheel tread designed by this method is subject to some restrictions. This method is suitable for vehicles running primarily on straight lines and/or with heavy traction forces, leading to a rapid change of wheel tread shape after the turning. Since the wheel profile designed by this method is for a specific rail profile, it has higher requirements for the running line. The designed wheel profile can only be used when the shapes of rails vary little.

(IV) Target normal gap method The vertical clearance (normal gap) between the wheel and the rail around the contact point is an important indicator for evaluating the compatibility of wheel/rail profiles, and a small normal gap can improve the "conformity" of the wheel and rail and reduce the contact stress, thereby reducing wheel wear. Based on this consideration, Cui et al. [26] proposed a wheel profile optimization method for reducing wheel wear based on target normal gap. In this method, three hypotheses are introduced: (1) the elastoplastic deformation of the wheel and rail is ignored; (2) the effect of wheelset yaw motion on the contact patch is ignored; (3) the flange thickness and height and wheel width remain is unchanged.

The first step of this method is to laterally move the wheelset, and the wheelset lateral distance is defined as Y_j, where j represents the j th contact point. Then the non-Hertzian contact method is used to solve the wheel–rail contact patch size of the contact point C_j, and c_1 and c_2 define the boundary of the calculated region, the values of which are set to be slightly larger than the corresponding semi-axis of the contact patch. As shown in Fig. 4, the normal gap function is defined as $D_j = \sum_{i=1}^{m} d_{ji}/m$, where d_{ji} is the normal clearance at the ith point and m is the number of discrete points in the region around the contact point C_j. Like the target RRD method [21], the ordinates z_j (j = 1, 2,…, n) of the movable points (see Fig. 2) are defined as design variables, which means that D_j can be represented by $D_j = D_j(Y_j, z_1, z_2, \ldots, z_n)$ since d_{ji} is determined by the wheel profile function $f(Y_j, z_1, z_2, \ldots, z_n)$. Finally, the objective function is introduced as

$$S = \frac{\sum_{j=1}^{K-1} c[w_j D_j(Y_j, z_1, z_2, \ldots, z_n) + w_{j+1} D_{j+1} Y_{j+1}, z_1, z_2, \ldots, z_n)]}{2} \rightarrow \min, \tag{4}$$

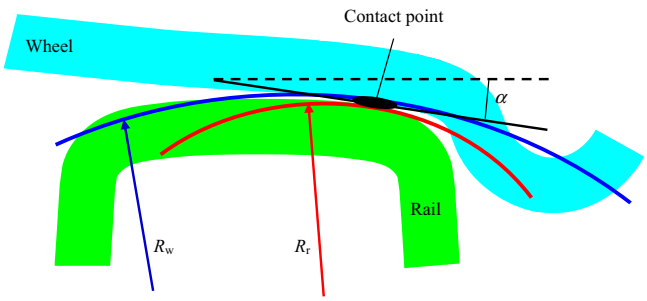

Fig. 3 Sketch of wheel/rail contact geometry

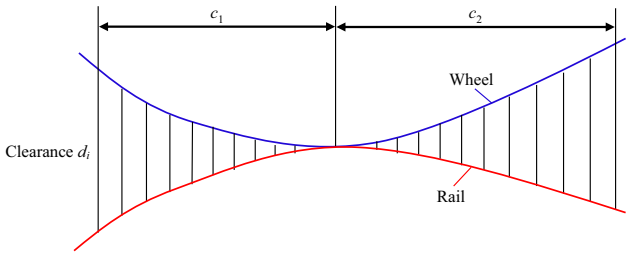

Fig. 4 Normal gap between the wheel and the rail

where K is the number of points in the normal gap curve, $c = |y_j - y_{j-1}|$, and w_j is a weighting factor. To ensure the safety of the vehicle and the monotonicity of the tread region of the generated wheel profile, some constraints to limit the equivalent conicity and slope are required [26].

In Ref. [26], this method was used to optimize the LMa wheel profile that matches the CHN60 rail. Simulation experiments showed that the curve-negotiation performance and wheel–rail contact stress level of the optimized profile are better than those of the traditional LMa profile. However, the effect of the wheelset yaw on the contact patch is not considered in this method, while some studies have shown that the wheelset yaw has a significant influence on the contact patch and wheel wear [28].

1.1.2 Multi-objective optimization methods

Compared with the single-objective optimization methods listed, the multi-objective optimization method has multiple objective (target) functions, and there is usually an interdependent relationship between the objective functions, even completely opposite or contradictory. The multi-objective optimization algorithm is to find a compromise in these relationships, thus multiple targets can be improved rather than one target improves and the other target deteriorates.

In the optimization of wheel profiles, the multi-objective optimization method is usually based on multi-body dynamics simulation (MBS). With the MBS technique, the dynamic responses corresponding to different wheel profiles can be obtained, and these wheel profiles are considered as the input of the optimization algorithm, and the dynamic responses are the output of the optimization algorithm. The output of the optimization algorithm often contains not only optimization targets, but also constraints. The frequently used outputs include wear index, RCF (rolling contact fatigue) index, safety-related index, stability-related index, noise index, comfort level, etc. It should be noted that when the number of the optimization target is 1, the multi-objective optimization problem is transformed into a single-objective optimization problem, which means that the multi-objective optimization method is also applicable to the single-objective optimization problem, an example is shown in Ref. [9]. In terms of the optimization algorithms, this section introduces two categories: (I) bio-inspired optimization algorithm and (II) response surface technique.

(I) Bio-inspired optimization algorithm The most common bio-inspired algorithm used to optimize wheel profiles is GA (genetic algorithm) [29]. For instance, Persson et al. [30] used GA to build the relationship between different wheel profiles and various dynamic parameters including ride comfort, lateral track-shifting force, maximum derailment coefficient, wear index, maximum contact stress, in which, 110 and 121 wheel profiles were generated for a soft bogie vehicle and a stiff bogie vehicle, respectively. Finally, a new wheel profile (P8) was obtained. Novales et al. [31] used GA to generate every new wheel profile through a semi-random combination of the fourth derivative (obtained in an incremental manner) of two wheel profiles of the last generation. In the formulation of optimization targets, a formula $I_T = d_f + 4T\gamma + I_{stress}$ that can transform a multi-objective optimization problem into a single-objective optimization problem was introduced, where d_f is the derailment coefficient, $T\gamma$ is the wear index, and I_{stress} is the wheel–rail contact stress. The formula can also be assigned with appropriate weights to consider factors such as track payout. Choi et al. [32] fitted 10 points, including five fixed points and five movable points (the same idea as in Fig. 2) by using a piecewise cubic Hermite interpolating polynomial function to generate new wheel profiles, and the corresponding wear index, surface fatigue index, maximum derailment coefficient, maximum lateral force, maximum overturning coefficient were calculated by the VAMPIRE software. Among them, the wear index and the surface fatigue index were designed as optimization targets, while the maximum derailment coefficient, the maximum lateral force, the maximum vertical force, and the maximum overturning coefficient were considered as boundary constraints. After that, the relationship between these generated profiles and wear index and surface fatigue index was established through NSGA-II (non-dominated sorting genetic algorithm, an improved GA). The final results showed that the optimized profile found by NSGA-II could reduce wear and fatigue, and yielded good performance in terms of derailment and lateral force.

Another classical bio-inspired algorithm that has been used in wheel profile optimization is the PSO algorithm [33]. For instance, based on the cubic NURBS (non-uniform rational b-spline) method, Lin et al. [34] applied PSO to design an LM thin flange wheel profile, in which, the wear index and wheel–rail lateral force were designed

as objective targets; the ordinate range, the tread monotonicity, the concave-convex properties, the flange thickness, and the derailment coefficient were designed as boundary constraints. However, the application of the thin flange wheel profile designed in Ref. [34] may involve modifications to existing designing or operating standards [35], thereby greatly reducing its versatility and engineering applicability. Cui et al. [36] used PSO to design a new wheel profile for a CRH1 train, in which, 14 movable points were designed as variables (see Fig. 2), and the generated wheel profile was fitted by using cubic spline function; a weighted function $f(z) = 10000w_1f_1 + w_2f_2 + 100w_3f_3$ was designed as the objective function, which considered the angle of attack f_1, the maximum lateral force f_2, and the carbody acceleration f_3, $w_i\,(i = 1, 2, 3)$ is the weighted factor; the tread monotonicity, the derailment coefficient, and the load reduction rate were designed as the constraints. Like Ref. [31], the study [36] also transformed the multi-objective optimization problem into a single-objective optimization problem.

Besides, there are also some other bio-inspired optimization algorithms that can be used in wheel profile optimization. For instance, Firlik et al. [37] applied CMA-ES (covariance matrix adaptation evolution strategy, a genetic approach) to design a wheel profile for a low-floor tram from the city of Poznań, Poland, in which, the wheel profile was divided into five parts (a cubic spline curve, an arc of a circle, a straight line and two fillets), and the spline curve was designed as the optimization region; the wear index, derailment coefficient, and contact area corresponding to over 50 000 wheel profiles were calculated. With the help of CMA-ES, an optimal wheel profile (FP7) was found.

(II) Response surface technique The basic idea of the response surface technique [38] is to locally adopt a low-order polynomial (quadratic or linear, this polynomial is often called a regression model) to fit a response surface that can reasonably reflect the real response (in wheel profile optimization, the target, and the constraints are the output responses). The optimization problem is solved by maximizing or minimizing the response surface. This method effectively reduces the amount of calculation through reasonable experimental design (such as sampling strategies). For instance, Ye et al. [9] used a small number of samples to build the relationship between wheel profiles and worn volume using KSM [39]. Through the established KSM, an optimized wheel profile to reduce wheel wear could be found. A similar study was presented in Ref. [40].

The biggest advantage of the methods based on bio-inspired algorithm and response surface technique is that they get rid of the establishment of a clear medium that reflects vehicle dynamics and wheel–rail contact mechanics, and directly find the relationship between the wheel profile and the optimization target through iterative calculation and/or regression calculation. In addition, these multi-objective optimization methods can also be applied to single-objective optimization problems, while the target-based techniques previously listed are inapplicable to multi-objective optimization problems. More importantly, by introducing multi-body dynamics models, these methods can accurately take vehicle-track system factors, including wheelset yaw and roll, track layout, etc., into account in the design of the wheel profile. However, it should be noted that these methods based on the bio-inspired algorithms are often computationally expensive since they involve a large number of iterative calculations, which means that a large number of MBSs are required.

1.2 Outlook

In addition to the aforementioned literature, there are also many other studies on wheel profile optimization [41–45]. Overall, the following outlook can be concluded:

(1) In terms of the design variables in multi-objective optimization methods, how to numerically represent the wheel profile is an important issue, such as arcs, fillets, straights, and splines. An expression that can well describe the profile of the wheel can not only reduce the amount of calculation but also the interface with MBS software is not error-prone.

(2) The selection of the objective function needs to be determined according to the train object. Freight trains are characterized by heavy axle load, and their running routes often contain many small-radius curves (such as the German Blankenburg–Rübeland railway line). The wheels are prone to fatigue, and the flange wear is often severe. The optimization targets should be more focused on safety and wheel damage. Passenger trains are characterized by fast speeds and people being transported, so their optimization targets should be more focused on safety, stability, and comfort. Of course, boundary constraints are essential.

(3) With the expansion of urbanization, more and more railway vehicles shuttle on fixed lines, such as metro, light rail, and tram [9]. In addition, due to some unique geographic or economic reasons, some vehicles typically operate on a designated line. For instance, some CRH1A and CRH380A trains only run on the China Hainan Roundabout Railway Line because of the unique island geography of Hainan province. For these vehicles shuttling on fixed lines, a specific wheel profile that takes into account the specific track layout is a good alternative.

(4) Bio-inspired algorithms require a large number of iterative calculations, and response surface techniques have regression capabilities. How to combine the two methods to quickly and reliably complete the task of optimizing wheel profiles, we believe this is a promising direction.

1.3 Contribution and structure of this work

The main work of this paper is summarized as follows:

(1) In Sect. 1.1, we briefly review the methods concerning wheel profile optimization over the past two decades.
(2) For the design of wheel profiles, we propose a comparably conservative rotary-scaling fine-tuning (RSFT) method to fine-tune the traditional wheel profiles, it is also an improvement of our previous work [9]. This method introduces two design variables and an empirical formula to generate new wheel profiles that meet the design standards. Besides, it avoids smoothing problems and has good compatibility with MBS software. More importantly, the new wheel profile obtained by fine-tuning the traditional profile is more proper to engineering applications.
(3) For the optimization method, we propose a KSM–PSO-based multi-objective optimization method. This method combines the iterative computing power of the bio-inspired algorithm with the regression capability of the response surface technique and can quickly and reliably complete the task of optimizing wheel profiles.
(4) We propose an RSFT–KSM–PSO method to optimize wheel profiles of railway vehicles shuttling on special lines, where a BOMBARDIER TRAXX locomotive serving on the German Blankenburg–Rübeland railway line is taken as a case to show how to implement the strategy.
(5) We propose two wear-resistant wheel profiles for the TRAXX locomotive serving on the Blankenburg–Rübeland railway line to reduce the severe flange wear we observed, and our preliminary results show that the two profiles satisfy the requirements specified in Standard UIC 518 [46], EN 14363 [47], EN 15313 [35], etc.

Section 2 of this paper introduces the RSFT method, where the profile S1002 is taken as an example to show how to generate new wheel profiles. In Sect. 3 we simulate the BOMBARDIER TRAXX locomotive and the Blankenburg–Rübeland railway line in SIMPACK. In Sect. 4, we propose a KSM–PSO-based multi-objective optimization method for optimizing wheel profiles. In Sect. 5 we present and analyze the simulation results. In Sect. 6 the improved wheel profiles are tested according to Standard EN 14363. This paper ends with a brief discussion and conclusions.

2 RSFT method for generating wheel profiles

An important step in wheel profile optimization is to generate new wheel profiles. As shown in Fig. 5, the current approaches for directly generating wheel profiles can be concluded into three main categories: (a) the approach based on fitting discrete points (FDP-approach), (b) the element combination approach, and (c) the scaling approach.

(a) Approach based on fitting discrete points: The wheel profile is firstly represented by discrete points (Fig. 5a). The points in the non-optimization region are fixed, while the points in the optimization region are movable within the constraints (usually the ordinate is movable). Then, these discrete points are connected by a curve fitting method to generate new wheel profiles. Some examples are given in Refs. [21–24, 26, 27, 32, 34, 37].
(b) Element combination approach: As plotted in Fig. 5b, the wheel profile is divided into several elements (sections), such as splines, arcs, and straights. Then, two (or more) elements act as the optimization region, and the parameters (e.g., the curvature of the circular arch, the length of the straight) of these elements are adjusted within constraints to generate a new wheel profile. A curve fitting method (e.g., B-splines, Beziers, NURBS) is generally required to ensure the smoothness of the generated wheel profile. An example is given in Ref. [44].
(c) Scaling approach: A scale factor α is introduced to enlarge or lessen the profile as a whole, as plotted in Fig. 5c. As mentioned in Ref. [9], the shortcoming of this approach is obvious, since a simple scale factor cannot take into account multiple indicators, such as safety-related index, stability-related index, wear index.

The first two approaches are promising, but they involve many design variables, which means that they are computationally expensive since a large number of iterative calculations and MBSs are required. More importantly, the setting of the curve is a complicated issue, which needs to consider wear, RCF, safety, stability, noise, comfort, service life, maintenance costs, etc. Since the performance shown in the face of these factors needs to be tested in long-term actual operation, a completely new wheel profile is difficult to be promoted for practical applications.

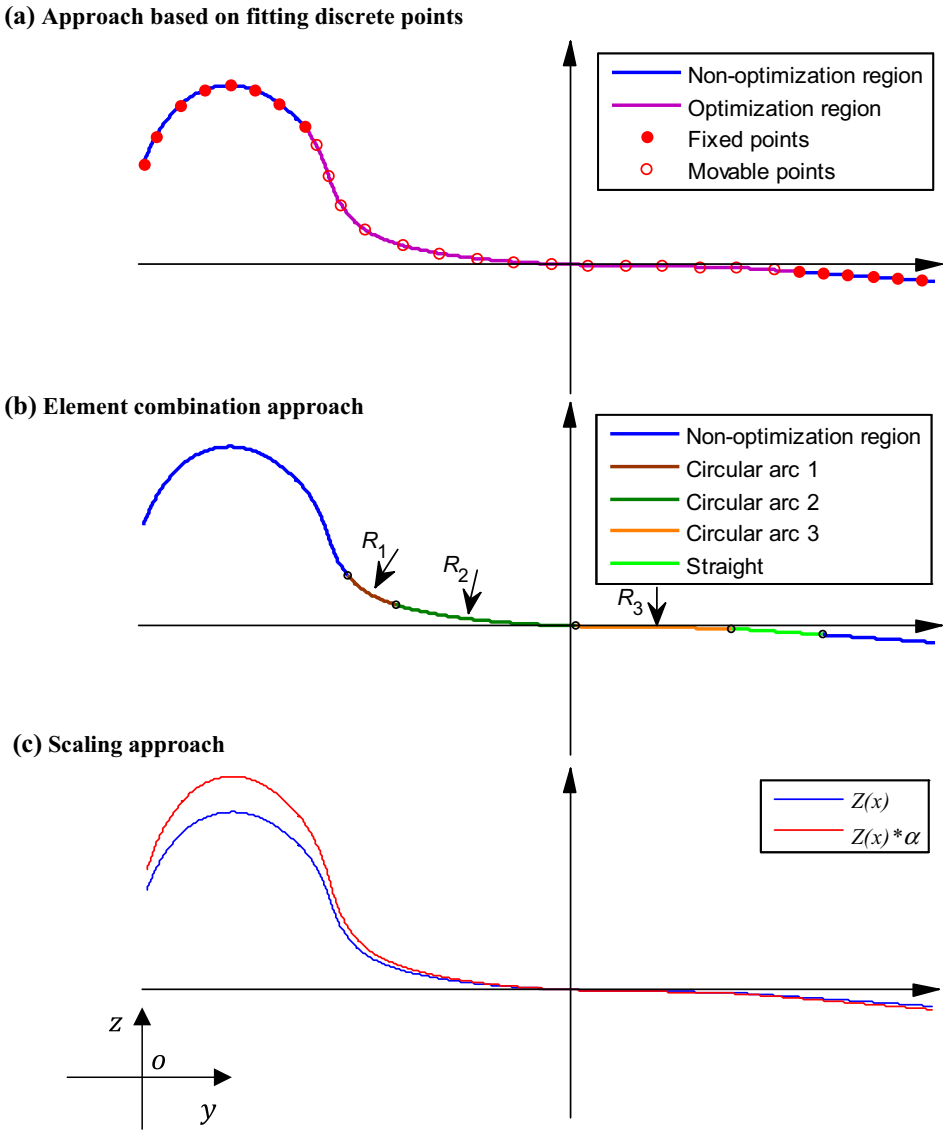

Fig. 5 Wheel profile generation approach

Alternatively, this paper introduces a comparably conservative RSFT method to fine-tune the traditional wheel profiles for improving their engineering applicability. Since the S1002 profile is a classic and widely used wheel profile in Europe and even worldwide [48], and it is also machined on the wheelsets of the introduced locomotive. It is, therefore, introduced as an example to show the theory and technique route of the RSFT method. The MATLAB code is disclosed in "Appendix 1" section. The specific steps, as shown in Fig. 6, are as follows:

Step 1 Rotation

The tread base point (nominal circle contact point) is set as the origin of the profile coordinate, and the lateral coordinate and vertical coordinate are set as oy-axis and oz-axis, respectively. The original S1002 is defined as a function of y, i.e., $z(y)$, and the point on the curve is written as (y, z). A transformation matrix $\boldsymbol{T}_1$ is introduced to rotate the curve until the vertex $A(y_\theta, z_{\max})$ of the curve coincides with the oy-axis and the point A after being rotated is written as A_1. The point (y, z) after being rotated is written as (y_1, z_1).

$$\begin{bmatrix} y_1 \\ z_1 \end{bmatrix} = \boldsymbol{T}_1 \begin{bmatrix} y \\ z \end{bmatrix}, \quad \text{and} \quad \boldsymbol{T}_1 = \begin{bmatrix} \cos\theta & \sin\theta \\ -\sin\theta & \cos\theta \end{bmatrix}, \tag{5}$$

where $\theta = \arctan(z_{\max}/y_\theta)$ is the rotation angle, $z_{\max}$ and y_θ are the ordinate and abscissa of point A, respectively.

Step 2 Scaling

The curve $z(y)$ after being rotated is written as $z_1(y)$, and a correction coefficient α_1 is introduced to scale the z-coordinate of the points on the curve:

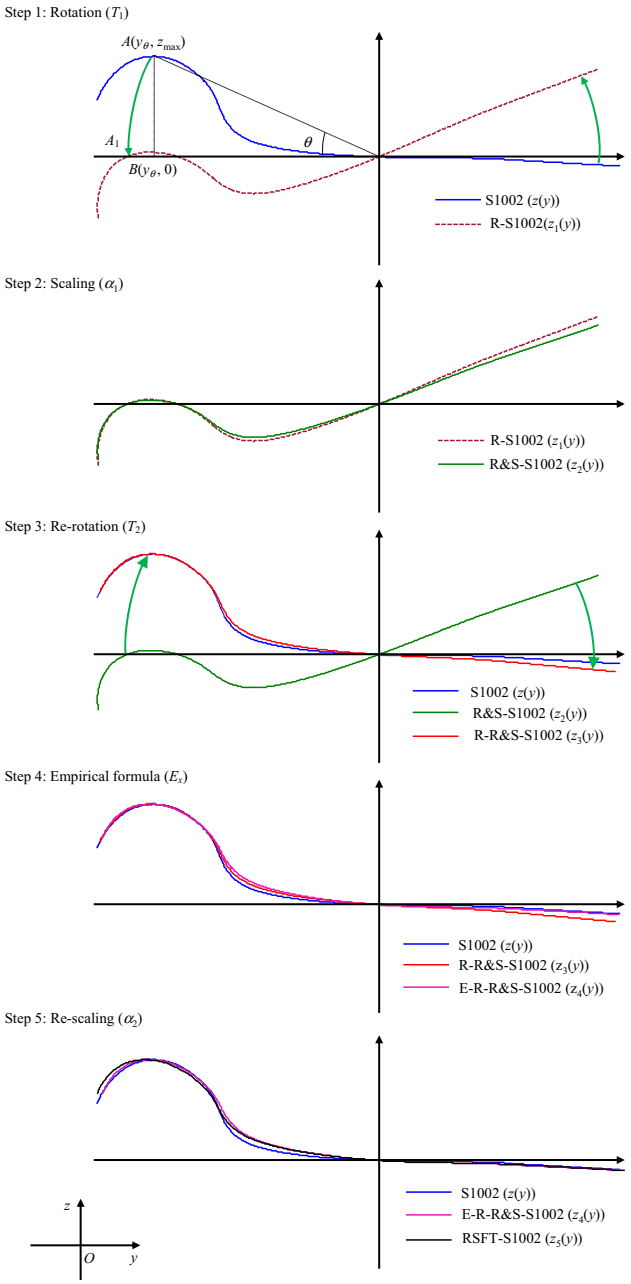

Fig. 6 RSFT method for wheel profile generation (an example of $\alpha_1 = 0.9$, and $\alpha_2 = 1.02$)

$$\begin{bmatrix} y_2 \\ z_2 \end{bmatrix} = \begin{bmatrix} y_1 \\ \alpha_1 z_1 \end{bmatrix}. \tag{6}$$

The selection of the value of α_1 needs to consider the following three issues: (1) A small change of α_1 significantly affects the equivalent conicity, and further affects the curve-negotiation performance and critical speed of the vehicle [49]. Besides, when the value of α_1 increases to 1.0561 (for the S1002 profile), the slope of the tread region is not strictly monotonic, which will worsen the self-centering ability of the wheelset. (2) Increasing or decreasing the value of α_1 affects the flange thickness S_d flange slope quota q_R, affecting the evaluation indicators (S_d and q_R in Fig. 7) specified in Standard EN 15313 [35] to a certain extent. (3) With reference to the North American transit system [50], the flange angle α_f is considered to vary within 60°–75°. Based on the above considerations, the value of α_1 is selected in the range of $0.95 \leq \alpha_1 \leq 1.05$.

Step 3 Re-rotation

A transformation matrix $\boldsymbol{T}_2 = \boldsymbol{T}_1^{\mathrm{T}}$, which is used to rotate the curve $z_2(y)$ back, is introduced to generate the curve $z_3(y)$, and the generated points (y_3, z_3) of $z_3(y)$, corresponding to (y, z) of $z(y)$, is expressed as

$$\begin{bmatrix} y_3 \\ z_3 \end{bmatrix} = \boldsymbol{T}_2 \begin{bmatrix} y_2 \\ z_2 \end{bmatrix}, \text{ and } \boldsymbol{T}_2 = \begin{bmatrix} \cos\theta & -\sin\theta \\ \sin\theta & \cos\theta \end{bmatrix}. \tag{7}$$

Step 4 Empirical formula

It can be seen from Fig. 6 (Step 3) that the adjusted profile $z_3(y)$ changes significantly in the inner section (left half axis) including the flange region. This section is the focus of optimization, as wear in this section is usually the most severe for vehicles running on curved tracks. However, the outer section (right half axis) also significantly changes. If one takes into account factors such as self-centering and critical speed, this section should be changed as little as possible, but not changing this section will cause the curve to be not smooth, deteriorating the running performance of railway vehicles. To solve this problem, an important empirical formula E_x is introduced to modify the curve, and the generated curve is written as $z_4(y)$

$$\begin{bmatrix} y_4 \\ z_4 \end{bmatrix} = \boldsymbol{T}_2 \begin{bmatrix} y_2 \\ z_2 - E_x \end{bmatrix}, \tag{8}$$

where E_x is obtained through our extensive simulation experiments, expressed as

$$E_x = \sin\left(\frac{\pi}{2}\frac{y_3}{|y_\theta|}\right) \cdot (z_3 - z), \tag{9}$$

y_θ is the abscissa corresponding to the vertex A of the S1002 profile, and z is the ordinate of the initial point on the original S1002 profile ($z(y)$). As shown in Fig. 6 (Step 4), the use of this formula produces the following three merits: (1) the inner section of the wheel profile can be adjusted to a large extent, while the outer section remains relatively stable, which can greatly reduce flange wear and ensure the self-centering ability of wheelsets; (2) the smoothness of the entire profile is guaranteed without

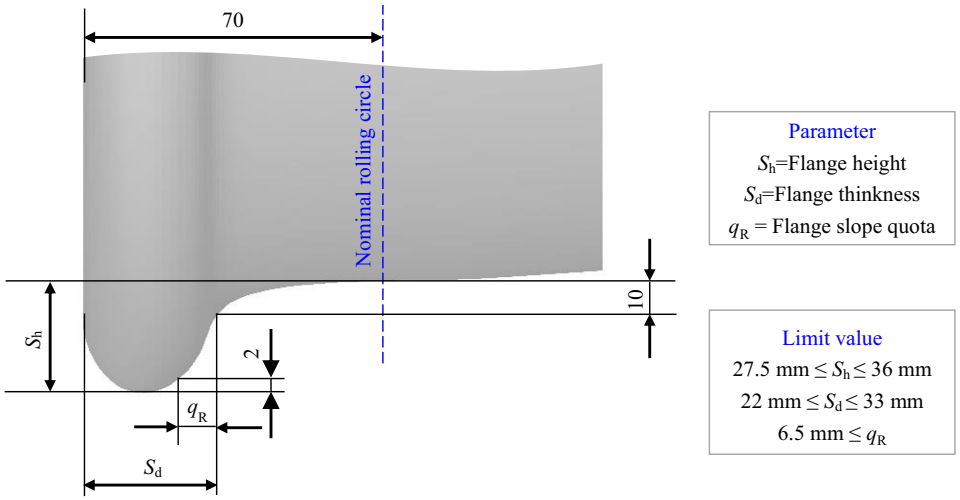

Fig. 7 Three parameters for evaluating wheel wear as well as their limits for a 1250-mm-diameter-wheel specified in EN15313

introducing a fitting function; and (3) the flange height remains constant and does not affect the evaluation index S_h specified in Standard EN 15313 [35].

Step 5 Rescaling

Another correction factor α_2 to scale the y-coordinates of these points (y_4, z_4) on the curve $z_4(y)$ is introduced to fine-tune the flange thickness, and the final curve is obtained as

$$\begin{bmatrix} y_5 \\ z_5 \end{bmatrix} = \begin{bmatrix} \alpha_2 y_4 \\ z_4 \end{bmatrix}. \tag{10}$$

It should be noted that a too-large or too-small value of α_2 may accelerate the other two indicators S_d and q_R specified in Standard EN 15313 [35] to reach the threshold for determining grinding, which will cause the wheelset to be scrapped in advance. Therefore, according to our experience, the range of α_2 is set as $0.98 \le \alpha_2 \le 1.02$. The determined design range of α_1 and α_2 ensures that the flange angle α_f changes within 60°–75°.

The proposed RSFT method only introduces two design variables, which greatly reduces the amount of calculation. Besides, the application of the empirical function can not only achieve the optimization of the flange region but also ensure the original ability of the wheelset when the vehicle runs on straight tracks. More importantly, based on the existing wheel profile, this method does not introduce a curve fitting method, avoids the complex curve design problem, and is easily generalized to engineering applications. However, it should be noted that this method relies heavily on the baseline model (the original wheel profile), and the superiority of the optimized profile depends to some extent on the baseline model.

3 Locomotive-railway line dynamics model

A TRAXX F140 AC locomotive from BOMBARDIER serving on the German Blankenburg–Rübeland railway line is taken as a case to show how to use the RSFT method to obtain an optimal wheel profile for wear reduction while meeting the requirements of operational safety.

3.1 BOMBARDIER TRAXX locomotive

The MBS model of the TRAXX locomotive simulated in our work consists of three sub-structures, one for the car-body and two for the bogies, where each bogie consists of one bogie frame, two motors, two motor hanging arms, two driven wheelsets, four axleboxes, and four axlebox arms. Like most locomotives, the TRAXX locomotive has two stages of suspensions, i.e., the primary suspension and the secondary suspension. The corresponding suspension elements are established as shown in Fig. 8a. Finally, the MBS model of the locomotive is made up of 35 rigid bodies, with a total of 130 degrees of freedom (DOFs). The final model simulated in SIMPACK is shown in Fig. 8b. Some data of interest are listed in Table 1. The unlisted data are confidential and the authors have no rights to disclose them.

3.2 Blankenburg–Rübeland railway line

The introduced TRAXX locomotive operated almost exclusively on the German Blankenburg–Rübeland railway line. This line was built starting in about 1880 in Blankenberge in the Harz Mountains, connecting the companies (such as Hüttenwerke and Kalkbranntwerke) there to the railway network [51]. On the one hand, bulk

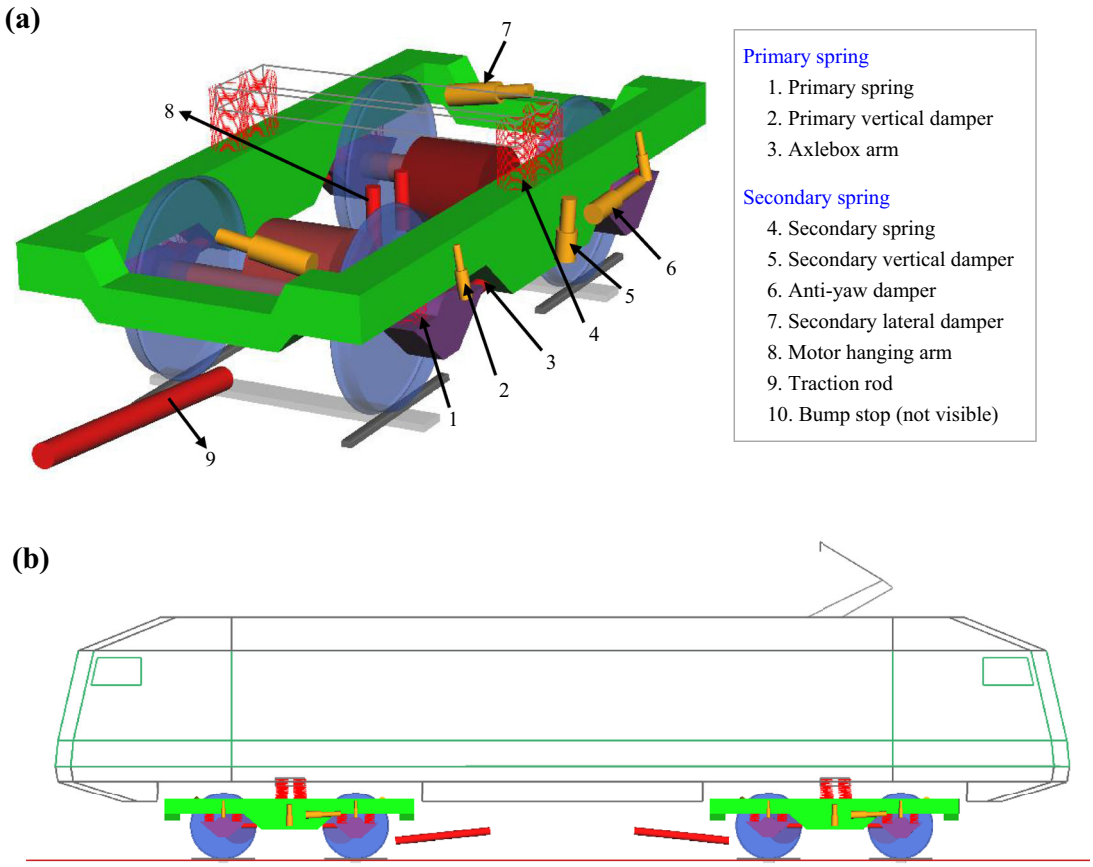

Fig. 8 Modeled elements of the suspension system (**a**) and the MBS model of the BOMBARDIER TRAXX locomotive (**b**)

Table 1 Related information of the locomotive-railway line model used in SIMPACK

Parameter	Value	Unit
Wheel arrangement	Bo–Bo	
Standard track gauge	1 435	mm
Distance between bogie centers	10,400	mm
Wheelbase	2600	mm
Wheel diameter (new)	1250	mm
Weight	83	t
Wheel–rail contact damping	10	kNs/m
Friction coefficient	0.35	
Poisson ratio	0.28	
Wheel profile	S1002	
Rail profile	UIC60E1	
Wheel–rail contact model	Hertzian contact + FASTSIM	
Track irregularity	ERRI B176	

goods must be transported away. On the other hand, raw materials such as coal and lime are supplied. Currently, most of the vehicles on this line mainly serve the lime project of the Fels-Werke GmbH in Harz. The corresponding transport route starts in Blankenberge and leads to Michaelstein before continuing to Rübeland. The return trip takes place in the reverse order, forming a cycle of the Rübelandbahn, with a total length of approximately 31.46 km. The satellite map of the line is shown in Fig. 9a.

The curvature, superelevation, and rail cant of the railway line are simulated according to the existing route plan [52, 53], and the track gauge S_w is approximately calculated by Eq. (11). Finally, the plan view of the line simulated in SIMPACK is shown in Fig. 9b. By comparing Fig. 9a with Fig. 9b, it can be known that the simulated line and the actual line are almost identical. The vehicle speed was measured by the authors' technique team [51]. For detailed technical information concerning the Rübeland–Blankenburg railway line, including the track layout parameters, as well as the vehicle speed, see our previous work [9].

$$S_{\mathrm{w}} = \begin{cases} 1.435 \text{ m, when } r_{\mathrm{arc}} = +\infty, \\ \dfrac{100}{r_{\mathrm{arc}}} \times 0.02 \text{ m} + 1.435 \text{ m, when } r_{\mathrm{arc}} \neq +\infty, \end{cases} \tag{11}$$

where r_{arc} is the arc radius.

4 KSM–PSO-based wheel profile optimization for wear reduction

4.1 Optimization problem statement

As can be seen from Fig. 9, the Blankenburg–Rübeland railway line has many tight curves, some of which even have a radius of only 180 m (see Ref. [9]), which results in severe wheel flange wear of vehicles shuttling on this line. In fact, this phenomenon has been confirmed in our previous project [51]. In this work, we aim to optimize the wheel profile of the TRAXX locomotives exclusively operating on this line to reduce wheel wear. Not only can it extend the service life of the wheelset, and it can also mitigate track deterioration.

4.1.1 Design variables and their limits

The correction factors α_1 and α_2 described in Sect. 3 are designed as the input variables of the optimization model, in which, α_1 and α_2 range in $0.95 \leq \alpha_1 \leq 1.05$ and $0.98 \leq \alpha_2 \leq 1.02$, respectively.

4.1.2 Optimization targets

The currently available wheel and/or rail wear models can be classified into two categories [54]: (1) the Archard-based models and (2) the $T\gamma$-based models. In the $T\gamma$-based models, such as the BRR model [55], the USFD model [56] and the Zobory model [57], the first step is to calculate the dissipated energy (wear number) in the wheel–rail contact patch. This is based on the assumption that there is a direct relationship between material loss and energy dissipation. In this paper, the energy dissipation is expressed as the product of the tangential force (T) and the creepage (γ), i.e., $T\gamma$:

$$T\gamma = F_x v_x + F_y v_y + M_z \varphi_z, \tag{12}$$

where F_x and F_y are longitudinal and lateral creep forces, respectively; v_x and v_y are longitudinal and lateral creepages, respectively; M_z and φ_z are the creep torque and spin creepage, respectively. Note that in SIMPACK 2020X the wheel–rail contact algorithm does not calculate the creep torque. Therefore, the wear number introduced here is the scalar product of the tangential forces and the related creepages.

The $T\gamma$ value of the first wheelset of the BOMBARDIER TRAXX locomotive driving from Blankenburg to Rübeland (approximate 15.73 km) is considered as the optimization target since the wheel–rail interaction force of the first wheelset is generally greater than that of the other wheelsets. Finally, the optimization targets are expressed as

$$\begin{cases} \text{Target 1: } w_{\mathrm{t}} = \int_{t_{\mathrm{s}}}^{t_{\mathrm{e}}} \left(T\gamma_{l.t}(t) + T\gamma_{\mathrm{r.t}}(t)\right) \mathrm{d}t \\ \text{Target 2: } w_{\mathrm{f}} = \int_{t_{\mathrm{s}}}^{t_{\mathrm{e}}} \left(T\gamma_{l.f}(t) + T\gamma_{\mathrm{r.f}}(t)\right) \mathrm{d}t \end{cases}, \tag{13}$$

where w_{t} and w_{f} are the total wear number of the tread region and flange region, respectively; t_{s} and t_{e} are the start and end simulation time, respectively; $T\gamma_{\mathrm{l.t}}(t)$ and $T\gamma_{\mathrm{r.t}}(t)$ are the $T\gamma$ value of tread region of the left and right wheel of the first wheelset, respectively; and $T\gamma_{\mathrm{l.f}}(t)$ and $T\gamma_{\mathrm{r.f}}(t)$ are the $T\gamma$ values of flange region of the left and right wheel of the first wheelset, respectively. With reference to Standard EN 13715 [58], in wear number calculation we consider the H2-C1* section and C1*-I section as the flange region and tread region, respectively, as shown in Fig. 10,

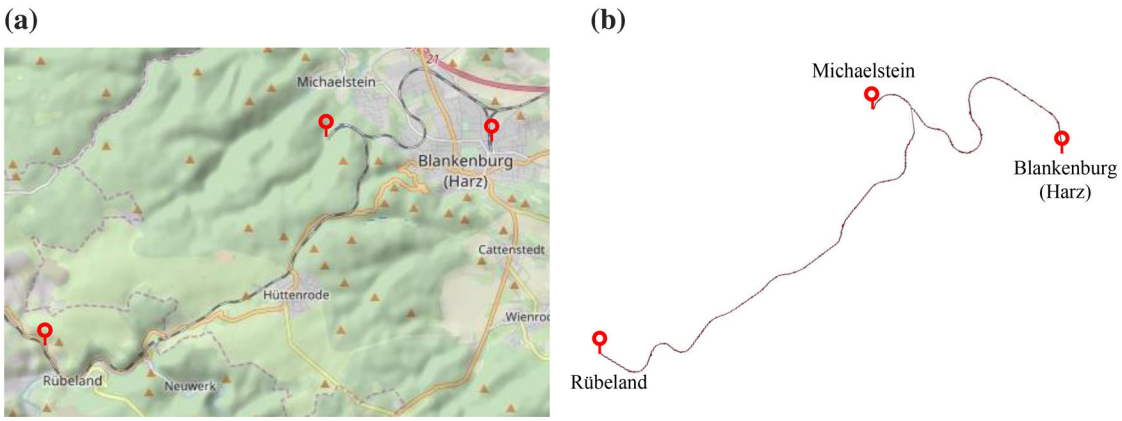

Fig. 9 Rübeland–Blankenburg railway line: **a** the satellite map, and **b** the plan view of the line simulated in SIMPACK [9]

where we define the coordinate of C1* as (− 26, zP), and zP is determined by the RSFD method introduced in Sect. 2.

4.1.3 Constraints

To guarantee the operational safety and stability, referring to Standard UIC 518 [46] and Ref. [32], the wheel–rail vertical force Q and Nadal's coefficient (derailment coefficient) f_d of all wheels, as well as the lateral force Y and overturning coefficient η of the vehicle system, among the whole line are designed as constraints.

Any high lateral force from the vehicle-track system, including wheel–rail lateral force and axlebox lateral force, is detrimental to the structural safety of the wheel and rail. Anyone of wheel–rail lateral force and axlebox lateral force (Y) must satisfy

$$Y|\max \le \frac{P_0}{3} + 10\,(\mathrm{kN}), \tag{14}$$

where P_0 is a static axle load.

A high vertical wheel–rail force may lead to severe wear and/or RCF on the track. The vertical wheel–rail force (Q) must satisfy

$$Q|\max \le 90 + Q_0\,(\mathrm{kN}), \tag{15}$$

where Q_0 is the static load on a wheel.

The derailment coefficient (f_d) is used to evaluate the safety of railway vehicles, and its permissible limit is

$$f_d = \frac{Y}{Q} \le 0.8. \tag{16}$$

The overturning coefficient (η) is an important index to evaluate the safety of railway vehicles, and its permissible limit is

$$\eta = \frac{\sum_{\text{bogie}} Q_{il} - \sum_{\text{bogie}} Q_{ir}}{\sum_{\text{bogie}} Q_{il} + \sum_{\text{bogie}} Q_{ir}} \le 1, \tag{17}$$

where Q_{il} and Q_{ir} are the vertical wheel–rail force on the left and right side of the ith wheelset, respectively.

Finally, the optimization problem is transformed into

$$\begin{cases} \text{Minimize: } w_t \\ \text{Minimize: } w_f \\ \text{Design varaible: } 0.95 \le \alpha_1 \le 1.05 \\ \text{Design varaible: } 0.98 \le \alpha_2 \le 1.02 \\ \text{Subject to: } Y \le 92.04\ \text{kN} \\ \text{Subject to: } Q \le 213.06\ \text{kN} \\ \text{Subject to: } f_d \le 0.8 \\ \text{Subject to: } \eta \le 1 \end{cases}. \tag{18}$$

4.2 KSM-based objective functions and constraint functions

For discrete datasets, parameter optimization is based on a large number of samples. Specifically, for the wheel profile optimization problem that relies on MBSs, the dynamic indexes corresponding to a large number of different profiles need to be evaluated, which means that a lot of repeated modeling and simulations are required. For example, in Ref. [37], to obtain a wheel profile that takes into account the wear index, the derailment coefficient, and the wheel–rail contact patch area, over 50 000 wheel profiles were evaluated. Such a huge number of simulations (or evaluations) that the railway industry is reluctant to do many deterministic analyses. Moreover, in our work, each simulation takes about three hours (computing facilities: software: SIMPACK 2020X; hardware: Intel Core i7-4790K, 4.00 GHz.), which is on the premise that the simulation can run smoothly. The calculation amount is so large that it is unrealistic to perform a large number of simulations. Therefore, it is of interest to introduce a high-

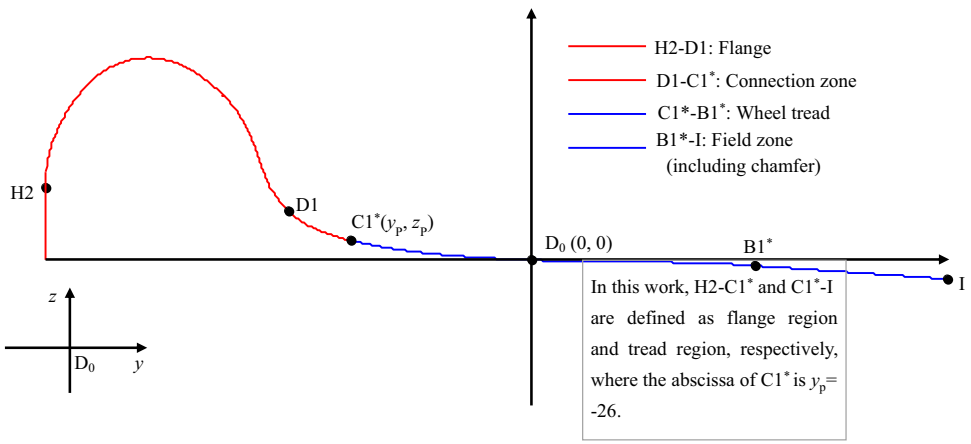

Fig. 10 Definition of the flange region and tread region (see EN 13715)

efficiency and reliable method to reduce the simulation amount.

KSM [39] is an interpolation technique based on statistical theory. It uses a small number of samples that meet a specific sampling strategy to construct a simplified mathematical model that approximates the original complex model. The essence of KSM is to perform regression or interpolation on the discrete dataset using an approximation function to predict the unknown region. This technique is introduced in our work to model the relationship between the correction factors (α_1 and α_2) and the wheel–rail wear number and constraints w_t, w_f, Y, Q, f_d, and η.

In the establishment of KSM, a group of $\left\{\alpha_1^{(i)}, \alpha_2^{(i)}, w_t^{(i)}, w_f^{(i)}, Y^{(i)}, Q^{(i)}, f_d^{(i)}, \eta^{(i)}\right\}$ is defined as the i th sample, $i = 1, 2, \ldots, n$, and n is the number of samples. The i th input design point is defined as

$$\boldsymbol{\alpha}^{(i)} = \left[\alpha_1^{(i)}, \alpha_2^{(i)}\right], i = 1, 2, \ldots, n, \tag{19}$$

where $\alpha_1^{(i)}$ and $\alpha_2^{(i)}$ are obtained by Latin hypercube sampling (LHS) strategy [59], and the corresponding output response point is defined as

$$\boldsymbol{r}^{(i)} = \left[w_t^{(i)}, w_f^{(i)}, Y^{(i)}, Q^{(i)}, f_d^{(i)}, \eta^{(i)}\right], \tag{20}$$

where $Y^{(i)}$, $Q^{(i)}$, and $f_d^{(i)}$ can be directly obtained in the SIMPACK post-processing file, while $w_t^{(i)}$ and $w_f^{(i)}$, and $\eta^{(i)}$ are calculated by Eq. (13) and Eq. (17), respectively. Therefore, the input dataset $\boldsymbol{A}$ and the output dataset $\boldsymbol{R}$ of KSM are, respectively, expressed as

$$\boldsymbol{A} = \begin{bmatrix} \boldsymbol{\alpha}^{(1)} \\ \boldsymbol{\alpha}^{(2)} \\ \vdots \\ \boldsymbol{\alpha}^{(n)} \end{bmatrix}, \boldsymbol{R} = \begin{bmatrix} \boldsymbol{r}^{(1)} \\ \boldsymbol{r}^{(2)} \\ \vdots \\ \boldsymbol{r}^{(n)} \end{bmatrix}. \tag{21}$$

Finally, the KSM-based objective functions and constraint functions are expressed as

$$\hat{r}(\boldsymbol{\alpha}) = f(\boldsymbol{\alpha})^{\mathrm{T}}\boldsymbol{\beta} + z(\boldsymbol{\alpha}), \tag{22}$$

where $\hat{r}(\boldsymbol{\alpha})$ is the predicted j th element of the vector $\boldsymbol{r}$, $j = 1, 2, \ldots, 6$; $f(\boldsymbol{\alpha})$ is a determined regression model, in our work, a quadratic polynomial regression model is applied; $\boldsymbol{\beta}$ is a vector of unknown coefficients of the regression model; $z(\boldsymbol{\alpha})$ a random process, in our work, a random Gaussian distribution is applied. Specifically, $\hat{r}_1(\boldsymbol{\alpha})$ and $\hat{r}_2(\boldsymbol{\alpha})$ are the objective functions, or written as $\widehat{w}_t(\boldsymbol{\alpha})$ and $\widehat{w}_f(\boldsymbol{\alpha})$; $\hat{r}_3(\boldsymbol{\alpha})$, $\hat{r}_4(\boldsymbol{\alpha})$, $\hat{r}_5(\boldsymbol{\alpha})$, and $\hat{r}_6(\boldsymbol{\alpha})$ are the constraint functions, or written as $\widehat{Y}(\boldsymbol{\alpha})$, $\widehat{Q}(\boldsymbol{\alpha})$, $\widehat{f}_d(\boldsymbol{\alpha})$, and $\widehat{\eta}(\boldsymbol{\alpha})$.

For a detailed description of KSM can be found in Ref. [39] or our previous work [60].

4.3 PSO-based optimization

After constructing the objective functions and constraint functions based on KSM, the optimal wheel profile for reducing wheel wear can be automatically sought by iterative optimization algorithms. Here PSO [33] is introduced, which mainly simulates the group foraging behavior of birds. In this method, the position of each particle represents a potential solution. The speed and direction of each particle are determined by its velocity vector, and the particle is randomly initialized to find the optimal solution by an iterative search. In each iteration, the velocity $\boldsymbol{v}$ and position $\boldsymbol{x}$ of the particles are updated by Eqs. (23)–(25)

$$\begin{aligned} v_{ij}(t+1) = {} & \omega_{t+1} v_{ij}(t) + c_1 r_{1j}(t)\left(p_{ij} - x_{ij}(t)\right) + \\ & c_2 r_{2j}(t)\left(p_{gj} - x_{ij}(t)\right), \end{aligned} \tag{23}$$

$$x_{ij}(t+1) = x_{ij}(t) + v_{ij}(t+1), \tag{24}$$

$$\omega_{t+1} = f_{\mathrm{damp}}\omega_t, \tag{25}$$

where t is the number of iterations, and is set as 100; $i = 1, 2, \ldots, N_p$, and N_p is the number of particles in the population, and is set as 100; $j = 1, 2, \ldots, N$, and N is the dimension of the solution space; ω_t is the weight, the initial value is set 1; f_{damp} is the damping coefficient to reduce ω_t after each iteration, and is set as 0.8; c_1 and c_2 are acceleration coefficients, both set as 2; r_{1j} and r_{2j} are random numbers that are uniformly distributed in 0–1; p_{ij} and p_{gj} represent the best positions found by particle and swarm, respectively. For a detailed description concerning PSO see Ref. [33].

5 Simulation

5.1 Technique route of the RSFT–KSM–PSO method

The RSFT–KSM–PSO-based wheel profile optimization method, as shown in Fig. 11, includes the following six steps:

Step 1 Select the correction factors α_1 and α_2 by the LHS method and construct the design variable matrix $\boldsymbol{A}$

Step 2 Generate wheel profiles corresponding to $\boldsymbol{A}$ according to the RSFT method introduced in Sect. 2

Step 3 Build the locomotive-railway line dynamics model in SIMPACK and run the simulation corresponding to each group of $\boldsymbol{\alpha} = [\alpha_1, \alpha_2]$, and obtain $[w_t, w_f, Y, Q, f_d, \eta]$

Step 4 Generate the required results including targets $[w_t, w_f]$ and constraints $[Y, Q, f_d, \eta]$ and construct the output response matrix $\boldsymbol{R}$ described in

Sect. 4.1. The simulated results are listed in "Appendix 2" section

Step 5 Build the relationship between $\boldsymbol{A}$ and $\boldsymbol{R}$ described in Sect. 4.2 by a response surface technique (the KSM technique)

Step 6 Search for the optimal combination of α_1 and α_2 for reducing wheel wear using PSO described in Sect. 4.3

5.2 Single-objective optimization

In order to visualize the whole process of the technique route described in Sect. 5.1, we first introduce the single-objective optimization problem. A total of 45 groups of design variables (correction factors) are selected, i.e., $n = 45$ in Eq. (19), as shown in Fig. 12a. Then, simulations corresponding to these correction factors are performed. The total wear number $w = w_t + w_f$ is set as the optimization target, i.e., $\boldsymbol{r} = [Y, Q, f_d, \eta]$ (Eq. (20)), and the relationship between $\boldsymbol{A}$ and $\boldsymbol{R}$ is established. The wear number responses $\boldsymbol{w}$ corresponding to the correction factors $\boldsymbol{A}$ are shown in Fig. 12b.

After bridging $\boldsymbol{A}$ and $\boldsymbol{R}$, we introduce a kind of surface response technique, KSM, to reflect the relationship between correction factors and total wear number, as shown in Fig. 12c. To ensure the correctness of the KSM–PSO method, the accuracy of KSM should be first guaranteed, where five groups of $\boldsymbol{\alpha}$ are randomly selected to run simulations. Table 2 compares the results calculated by the established KSM and the ones simulated in SIMPACK. All the errors are less than 4%, which shows that the established KSM is accurate enough and can be considered as the objective function of PSO.

Finally, the optimal combination of α_1 and α_2 for reducing wheel wear is found by PSO, as shown in Fig. 12d. It can be seen that when the value of $\boldsymbol{\alpha} = [1.036, 1.0067]$, the total wear number is the smallest, which is 7.2394×10^3 kN and the corresponding wheel profile is called S1002-S. The comparison between the S1002 and S1002-S profiles is shown in Fig. 13. It can be seen that the inner section of the wheel, including the flange region, changes obviously, while the outer section remains almost unchanged. In order to prove the superiority of the S1002-S profile, the related results of the S1002 profile calculated by KSM are introduced for comparison, as listed in Table 3. It can be known that when using the S1002-S profile, the total wear number is reduced by 30%, while other parameters related to stability and safety are hardly affected.

Two points need to be explained here:

(1) It should be noted that the S1002-S profile found by PSO may not be the optimal one that minimizes the total wear number, as this process is disturbed by the errors of the established KSM. As can be seen from the color map of Fig. 12d, when the value of α within the red rectangle, all the corresponding wheel profiles can greatly reduce the total wheel number. Therefore, from the perspective of reducing the total wear number, all the wheel profiles derived from the red rectangle can be considered as an alternative.

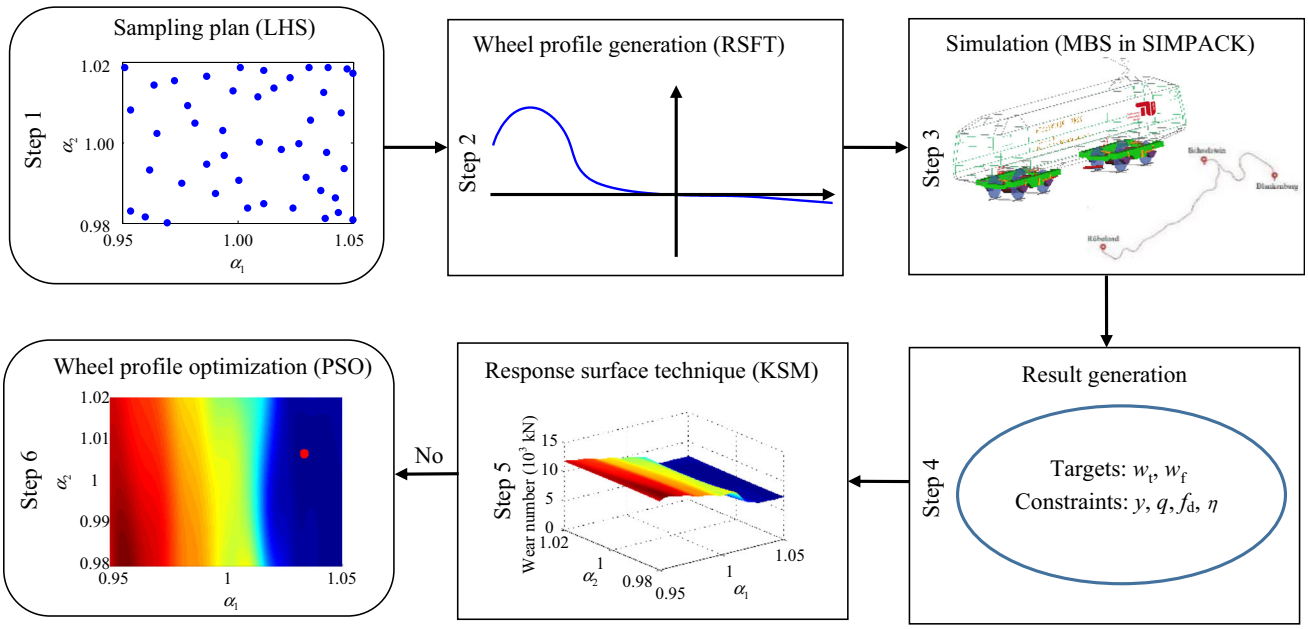

Fig. 11 Steps of the RSFT–KSM–PSO method for wheel wear reduction

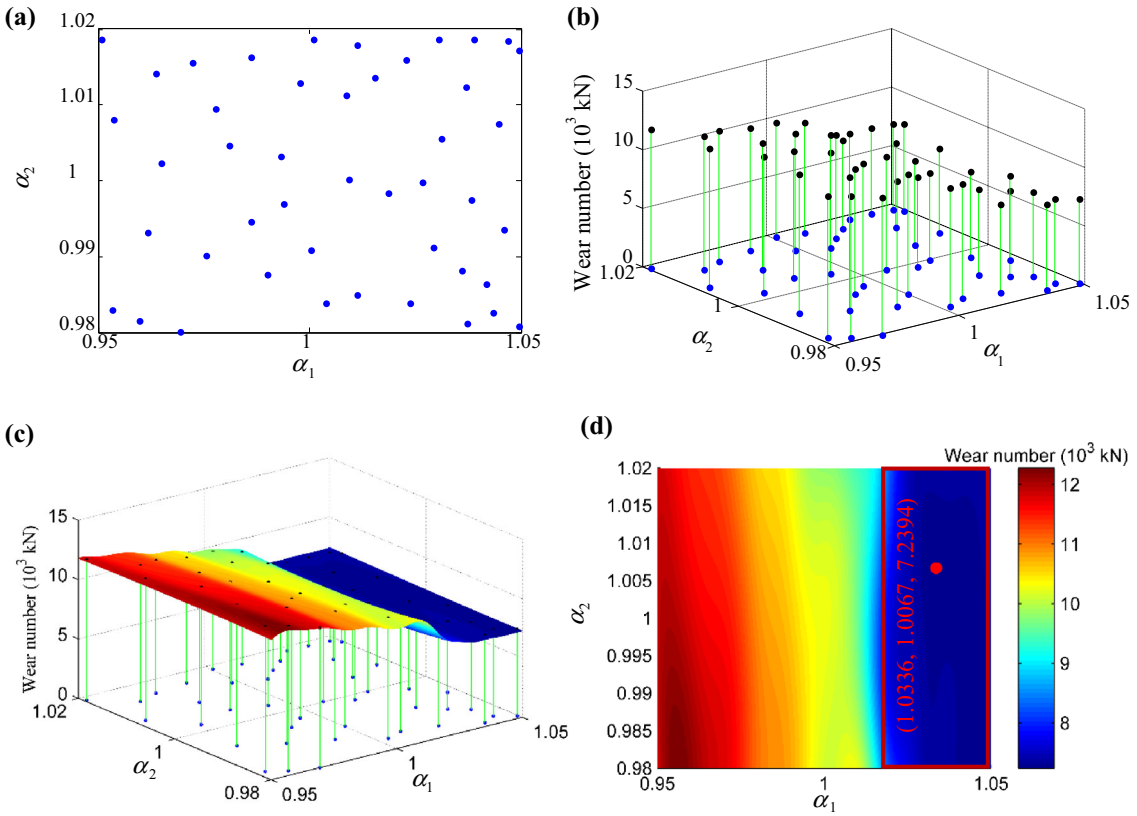

Fig. 12 Input sample variables (**a**), output sample responses (**b**), the corresponding KSM model (**c**), and the optimal result solved by PSO (**d**)

Table 2 Comparison between the results calculated by KSM and the results simulated in SIMPACK

Correction factor α	Total wear number calculated by KSM w ($\times$ 10^3 kN)	Total wear number simulated in SIMPACK w ($\times$ 10^3 kN)	Error (%)
[0.9698, 1.0140]	11.3224	11.3186	− 0.34
[0.9758, 0.9955]	11.2902	11.2773	− 1.14
[1.0110, 1.0080]	9.4535	9.4830	3.11
[1.0330, 0.9870]	7.3231	7.3356	1.99
[1.0400, 1.0120]	7.2721	7.2632	− 1.22

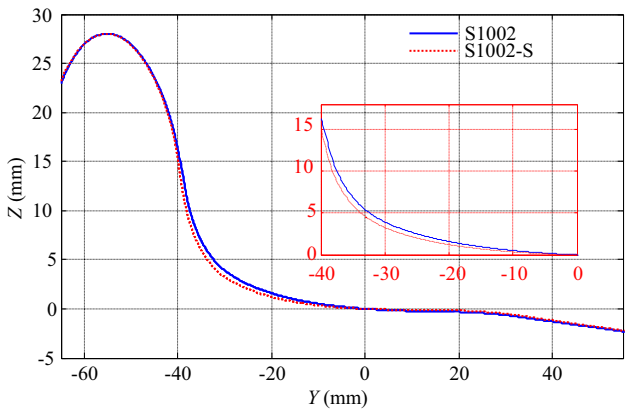

Fig. 13 Comparison between the S1002 and S1002-S profiles

(2) From Fig. 12d, it can be seen that changing α_1 significantly affects the wear number, but changing α_2 has a relatively small effect on the wear number, which means that the value of α_2 can be selected within the range of $0.98 \leq \alpha_2 \leq 1.02$. From the

Table 3 Comparison of results calculated by KSM

Wheel profile	α	w ($\times$ 10^3 kN)	Y (kN)	Q (kN)	f_d	η
S1002	[1.0000, 1.0000]	10.3386	69.885	137.81	0.5150	0.1487
S1002-S	[1.0336, 1.0067]	7.2394	67.780	137.88	0.5022	0.1484

maintenance point of view, to ensure that the flange thickness (S_d shown in Fig. 7) of the adjusted profile does not change, it is recommended to determine the value of α_2 according to the value of α_1, i.e., by changing α_2 to compensate for the increase or decrease in the flange thickness caused by the change of α_1. The optimal relationship between α_1 and α_2 will be studied in our future work.

5.3 Multiple objective optimization

To study the optimal relationship between the tread wear and the flange wear, we introduce a multi-objective optimization strategy. The tread wear number w_t and flange wear number w_f are set as the optimization targets, i.e., $\boldsymbol{r} = [w_t, w_f, Y, Q, f_d, \eta]$ [Eq. (20)]. According to the steps described in Sect. 5.1, 100 Pareto solutions are obtained, as shown in Fig. 14. These Pareto solutions reflect a nearly linear relationship between the tread wear number and the flange wear number, i.e., reducing the flange wear number will increase the tread wear number.

Generally, the flange wear has the greatest impact on the safety of railway vehicles, and the resulted grinding depth is often deeper. Therefore, flange wear should be avoided as much as possible. The S1002-S profile obtained through the single-objective optimization in Sect. 5.2 is the profile that causes the least flange wear number. Therefore, in the multi-objective optimization, we select a compromise between tread wear number and flange wear number (the red point in Fig. 14, where $\boldsymbol{\alpha}$ = [1.0195, 1.0151]) as a case for analysis, and the corresponding wheel profile is called S1002-M.

The comparison between the S1002 and S1002-M profiles, as well as the dynamic parameters calculated by KSM, are shown in Fig. 15 and listed in Table 4, respectively. It can be seen that when the S1002-M profile is used, a proper sacrifice of the tread wear number can greatly reduce the flange wear number, and the total wear number is also reduced. In the example in this section, the tread wear number has been increased by 16%, while the flange wear number and the total wear number is reduced by 65% and 21%, respectively. In addition, the results listed in Table 4 show that the dynamic performance is not sacrificed.

5.4 Long-term wear comparison between the S1002, S1002-S, and S1002-M profiles

Through the above RSFT–KSM–PSO method, it can be known that the S1002-S and S1002-M wheel profiles are advantageous in terms of short-term wear numbers for the BOMBARDIER TRAXX locomotive serving on the German Blankenburg–Rübeland railway line. To further prove that the improved wheel profiles are still superior to the standard S1002 profile in the long-term wear process, a wear distribution calculation method that integrates the Hertzian normal contact model [61], FaStrip tangential contact model [62], and USFD wear model [56] (i.e., Hertzian-FaStrip-USFD [9, 63]) is introduced to calculate the wheel wear distribution of the TRAXX locomotive after driving 1573 km. The theory of the Hertzian-FaStrip-USFD method and the selection of parameters can be found in our previous work [9].

Figure 16 shows the average wear distribution of the eight wheels of the locomotive under different wheel profiles. From this figure, the following observations are found:

(1) When using the S1002 wheel profile, the wear depth of the flange is very large, and the wear distribution is extremely uneven.
(2) When using the S1002-S wheel profile, the wear depth of the flange is greatly reduced, while the wear depth of the tread is obviously increased.
(3) When using the S1002-M wheel profile, the wear depth of the tread decreases slightly. More

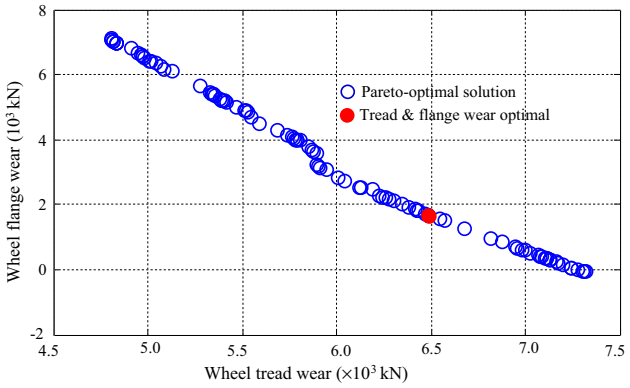

Fig. 14 Multi-objective optimization results by KSM–PSO

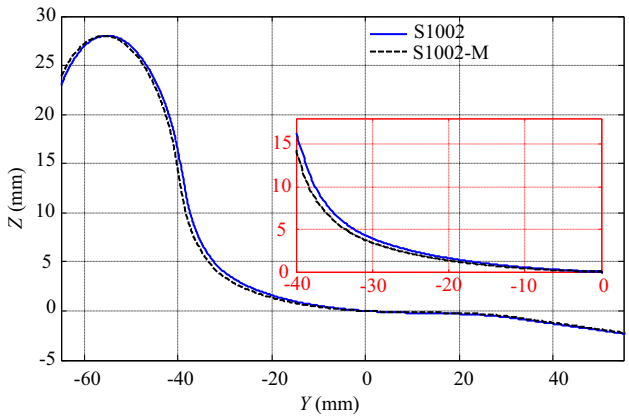

Fig. 15 Comparison between the S1002 and S1002-M profiles

Table 4 Comparison of results calculated by KSM

Wheel profile	α	w_t ($\times 10^3$ kN)	w_f ($\times 10^3$ kN)	Y (kN)	Q (kN)	f_d	η
S1002	[1.0000, 1.0000]	5.5886	4.7500	69.885	137.81	0.5150	0.1487
S1002-M	[1.0195, 1.0151]	6.4870	1.6762	68.081	137.87	0.5093	0.1491

importantly, the wear depth of the flange decreases significantly and the wear distribution is more uniform.

The above observations show that wheel wear can be reduced when using the improved wheel profiles (S1002-S and S1002-M). Particularly, flange wear can be significantly reduced. To account for this, Fig. 17 presents the RRD, equivalent conicity, and contact distribution of the S1002, S1002-S and S1002-M profiles when the track gauge is 1.435 m with a rail cant of 1/40. It can be seen that compared with the S1002 profile, the S1002-S and S1002-M profiles have better curve-negotiation capabilities since the flange contact generates larger lateral displacement on the curved track, while the optimized profiles show similar performances on the tangent track due to little changes of the tread section. Similar conclusions and explanations can be found in Ref. [23, 24, 32].

The long-time wear simulation proves that the improved wheel profiles are advantageous in terms of wear reduction, which further proves the correctness of the RSFT–KSM–PSO method, and meanwhile illustrates that this method is promising for practical engineering.

6 Quasi-static and hunting stability tests

Before putting into use, the improved wheel profile must satisfy the requirements specified in the acceptance standard EN 14363 [47]. Due to the huge workload, in this work, we only present the quasi-static safety against derailment on a twisted track and the hunting stability on a straight track.

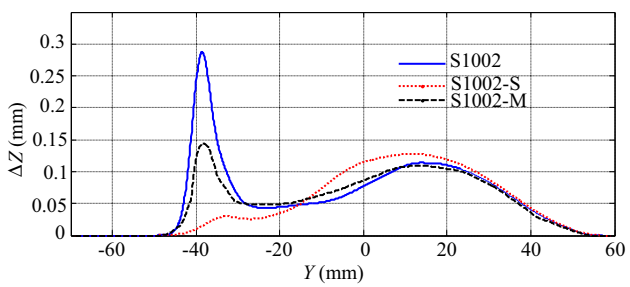

Fig. 16 Comparison of wear distribution of the S1002, S1002-S, and S1002-M profiles

6.1 Quasi-static safety against derailment on twisted track

We carry out the quasi-static test in accordance with Method 1 specified in EN 14363. The vehicle must negotiate a 150-m-radius twist track without the wheel lift of the outer leading wheel exceeding 5 mm. For this purpose, we built a twisted track with a gauge of 1460 mm. The track layout, including radius (R) and superelevation (H) distributions, is shown in Fig. 18a, b, the track consists of the following sections:

- a straight line of 11 m,
- a 100-m-long transition curve with the end radius of 150 m,
- a 430-m-long full arch with a radius of 150 m,
- and a straight line of 30 m.

The twist g is determined by the wheelbase distance and the pivot distance between bogies, where we used a constant twist of $g_0 = 3^0/_{00}$. The twist deficiency is balanced by the additional "gaskets" added under the primary- or secondary springs. EN 14363 [47] provides detailed information concerning this section, and a simple acceptance case can be found in our previous work [64].

The evaluation criterium is the maximum value ΔZ_{max} of the wheel lift of the curve-outer wheel of the leading wheelset. The limit value is $\Delta Z_{max} < \Delta Z_{lim} = 5$ mm. As shown in Fig. 18c, although the two wear-resistant wheel profiles have a slight increase in wheel lift on the twisted curved track, they are well below the limit value. In addition, the Y/Q ratio is introduced as an auxiliary evaluation index. Figure 18d shows that the Y/Q ratio of the two wear-resistant wheel profiles is almost the same as that of the S1002 profile, and all are below 1.2.

6.2 Hunting stability

We carry out the hunting stability assessment by estimating the nonlinear critical speed using the deceleration method [65] with an acceleration of -0.3 m/s^2. The simulation runs in Fig. 19 show that the critical speed of profile S1002 is about 335 km/h, while that of the two wear-resistant wheel profiles is slightly lower, about 314 km/h for S1002-S and 326 km/h for S1002-M, respectively. However, for

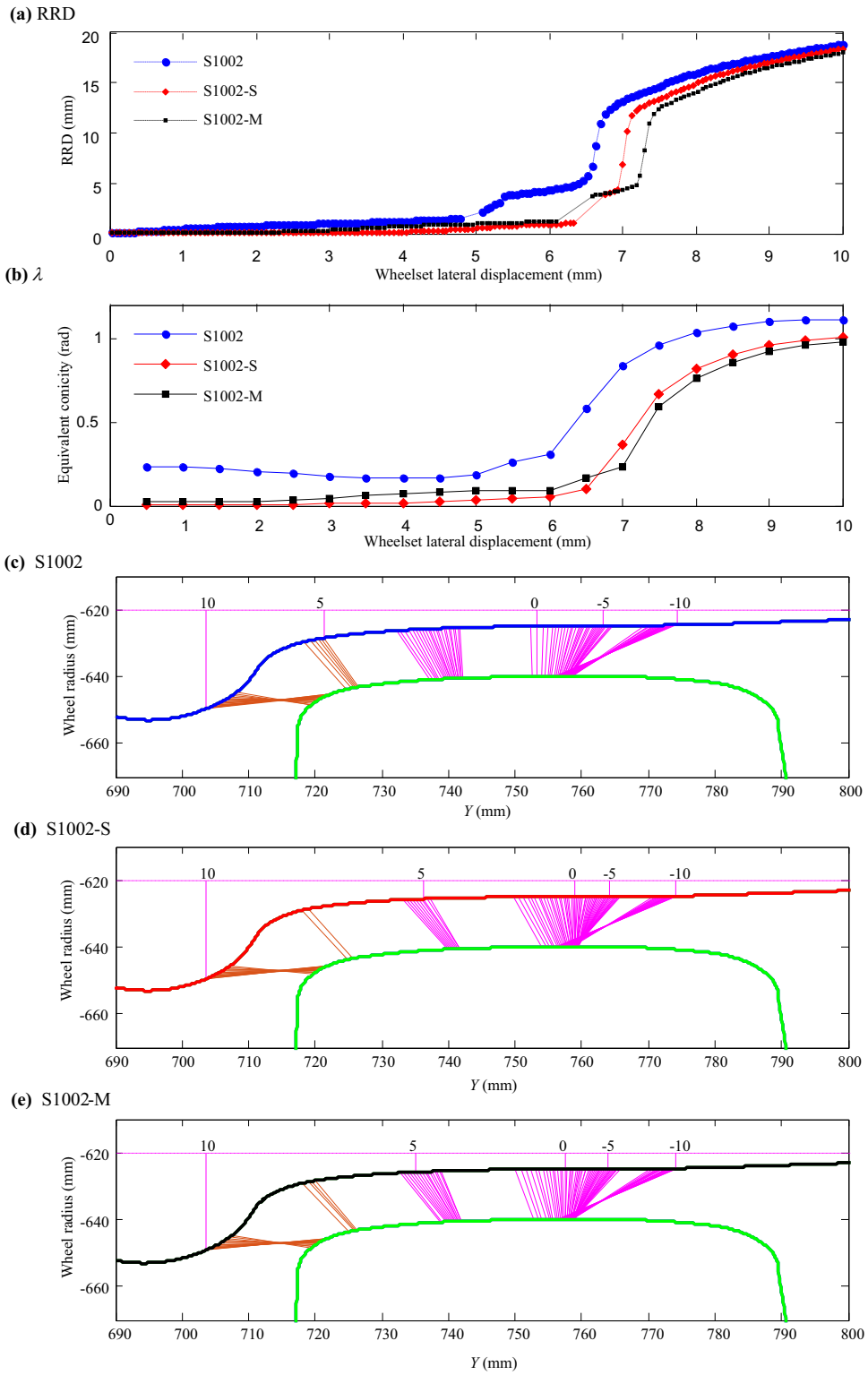

Fig. 17 RRD (**a**), equivalent conicity (**b**), and contact distribution (**c**–**e**) of the S1002, S1002-S, and S1002-M profiles

freight vehicles the slight reduction is acceptable since the critical speed of 314 km/h is usually considerably higher than the actual running speed. For instance, the maximum speed of the TRAXX locomotive on the Blankenburgen-burg–Rübeland railway line usually does not exceed 60 km/h.

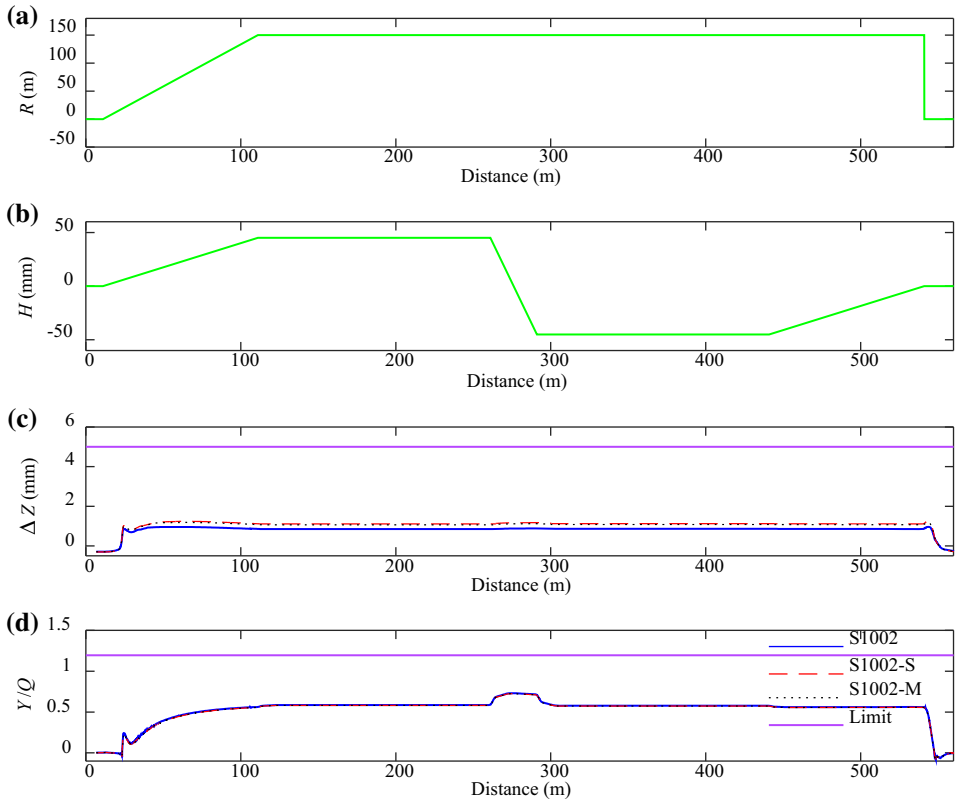

Fig. 18 Track layout of radius (**a**) and superelevation (**b**) according to EN 14363 and comparison of wheel lift (**c**) and derailment quotient Y/Q (**d**) between the S1002, S1002-S and S1002-M profiles

7 Conclusion and discussion

Currently, the multi-objective wheel profile optimization methods mainly include three sub-modules: (1) the formulation of design variables to generate wheel profile curves, (2) the dynamic simulation to obtain the relationship between the design variables and the dynamic performance, and (3) the selection of the optimization algorithm to find the optimal wheel profile. In this article, the work on these three modules is briefly summarized as follows:

(1) In terms of the first module, we propose a comparably conservative RSFT method to fine-tune the traditional wheel profiles. Compared with the approach based on fitting discrete points and the element combination approach, the RSFT method introduces only two design variables, which greatly reduces the amount of calculation. Besides, the empirical function applied in this method can not only achieve the optimization of the flange region but also ensure the original ability of the wheelset when the vehicle runs on a straight line. More importantly, based on the existing wheel profile, this method does not introduce a curve fitting method, avoids the complex curve design problem, and is easily generalized to engineering applications.

(2) In terms of the second module, for the BOMBARDIER TRAXX locomotives serving on the German Blankenburgenburg–Rübeland railway line, we build a KSM-based function to reflect the relationship between the wheel profile designed by the RSFD method and the wheel–rail wear number.

(3) In terms of the third module, we propose a KSM–PSO-based optimization method. This method combines the iterative computing power of the bio-inspired algorithm with the regression capability of the response surface technique and can quickly and reliably complete the task of optimizing wheel profiles.

(4) With the RSFT–KSM–PSO method, we present two wear-resistant wheel profiles for the TRAXX locomotives serving on the German Blankenburgenburg–Rübeland railway line, namely S1002-S and S1002-M. The S1002-S profile minimizes the total wear number by 30%, while the S1002-M profile makes the wear distribution more uniform through a proper sacrifice of the tread wear number, and the total wear number is reduced by 21%. Our preliminary results

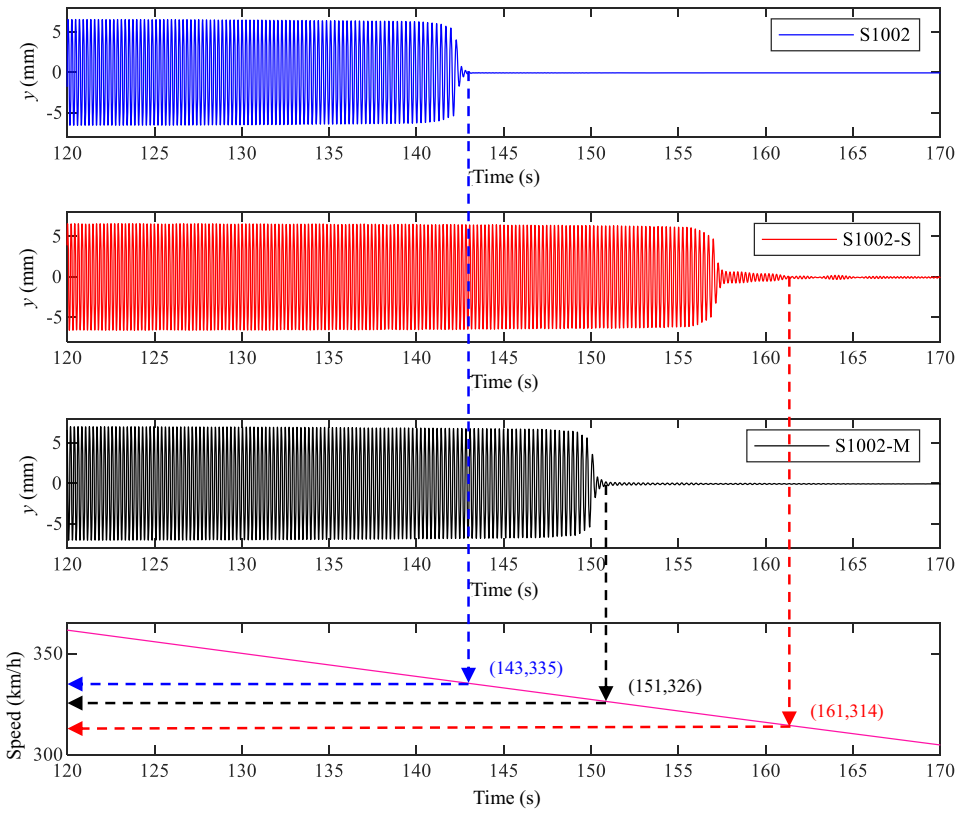

Fig. 19 Simulation runs of S1002, S1002-S and S1002-M through the deceleration method

show that the two wear-resistant wheel profiles meet the requirements specified in standards UIC 518, EN 14363, EN 15313, etc.

The article ends with the following three points: (1) The coupler forces on freight locomotives of a long heavy-haul train are very large, which could greatly affect the locomotive dynamics and wheel wear. However, we have not considered the coupler forces in this paper. (2) It should be noted that the RSFT method relies heavily on the baseline model (the original wheel profile), and the superiority of the optimized profile depends to some extent on the baseline model. (3) We are studying the performance of this method in metros, and the relevant information will be reported in our future work.

8 Replication of results

The unlisted data about the locomotive and the railway line are confidential and the authors have no rights to disclose them. Readers interested in the MATLAB code and the internal reports are encouraged to contact the corresponding authors by E-mail. The RSFT algorithm and the original simulated results from SIMPACK are disclosed in "Appendices 1 and 2" section, respectively.

Acknowledgements This work is supported by the Assets4Rail Project which is funded by the Shift2Rail Joint Undertaking under the EU's H2020 program (Grant No. 826250) and the Open Research Fund of State Key Laboratory of Traction Power of Southwest Jiaotong University (Grant No. TPL2011), and part of the experiment data concerning the railway line is supported by the DynoTRAIN Project, funded by European Commission (Grant No. 234079). The first author is also supported by the China Scholarship Council (Grant No. 201707000113).

The authors would like to thank Prof. Dr. Oldrich Polach and Dr. Henning Schelle for the support. Thank Spree River, the "Vaterfluss" of Berlin, which inspired the author when he was jogging along the path beside and brought him the idea of the RSFT-based wheel profile generation method proposed in this paper.

Appendix 1: MATLAB code of the RSFT algorithm

```
%%%% This MTALAB code (RSFT method) is used to adjust the two correction factors
for the S1002 (or any other) wheel profile for optimization purpose %%%%
% Ref.: Rotary-scaling fine-tuning (RSFT) method for optimizing railway wheel profiles
and its application to a locomotive %
% 19.03.2020 %
%
%%% Start %
Profile=load('S1002.txt'); % Unit in m
Profile=Profile*1000; % Unit in mm
y=-70:0.1:60;
z=interp1(Profile(:,1),Profile(:,2),y);
S1002=[y' z'];
[m,index]=max(Profile(:,2));
theta=-atan(m/abs(Profile(index,1)));
%% Step 1
T1=[ cos(theta) sin(theta)
      -sin(theta) cos(theta)]; % Transformation Matrix
for i=1:length(Profile(:,1));
    Profile_1(i,:) = T1*[Profile(i,1);Profile(i,2)];
end
%% Step 2
alpha1=1.0336; % Correction factor, ranges in 0.95-1.05 for Profile S1002
Profile_2(:,1)=          Profile_1(:,1);
Profile_2(:,2)=alpha1*Profile_1(:,2);
%% Step 3
T2=[ cos(theta) -sin(theta)
      sin(theta) cos(theta)]; % Transformation Matrix
for i=1:length(Profile(:,1));
    Profile_3(i,:) = T2*[Profile_2(i,1);Profile_2(i,2)];
end
%% Step 4
for i=1:length(Profile(:,1));
    y_theta=Profile(index,1);
    delta=Profile_3(i,2)-Profile(i,2);
    Ex=delta*sin((pi/2)*Profile_3(i,1)/abs(y_theta));
    Profile_4(i,:) = T2*[Profile_2(i,1);Profile_2(i,2)-Ex];
end
%% Step 5
alpha2=1.0067; % Correction factor, ranges in 0.98-1.02 for Profile S1002
Profile_5(:,1)=alpha2*Profile_4(:,1);
Profile_5(:,2)=          Profile_4(:,2);
%% Figure
plot(Profile(:,1),Profile(:,2),'b')
hold on
plot(Profile_5(:,1),Profile_5(:,2),'k')
xlabel ('Y (mm)','FontName','Times New Roman','FontSize',11);
ylabel ('Z (mm)','FontName','Times New Roman','FontSize',11);
axis ([-65,55,-5,30])
set(gcf,'Position',[500,262,600,250]);
% END %%%
```

Appendix 2: Design variables and the corresponding simulated results from SIMPACK

Design variables		Simulated results					
α_1	α_2	w_t (N)	w_f (N)	Y (N)	Q (N)	f_d	η
0.9537	1.0080	4,844,100	7,051,550	70,772	137,925	0.527417	0.149963
1.0418	0.9863	7,250,800	26,208	68,250	137,839	0.502634	0.147265
1.0227	1.0160	6,938,625	732,832	67,746	137,812	0.507786	0.149098
0.9933	1.0031	5,530,275	4,842,115	69,917	137,800	0.517167	0.148922
1.0111	0.9850	5,819,325	3,964,806	69,589	137,612	0.514799	0.147625
1.0087	1.0113	5,827,800	3,859,997	69,065	137,896	0.512280	0.149120
1.0154	1.0137	6,027,300	2,848,818	68,525	137,927	0.510027	0.149106
1.0185	0.9983	6,874,775	920,251	68,535	137,720	0.510763	0.148103
0.9616	0.9931	4,910,675	6,936,134	70,788	137,780	0.527682	0.149046
0.9650	1.0023	4,996,950	6,584,684	70,609	137,858	0.525471	0.149460
0.9899	0.9875	5,384,025	5,356,788	70,059	137,621	0.520661	0.148166
0.9694	0.9800	4,984,275	6,787,084	70,784	137,627	0.527736	0.148209
0.9723	1.0155	5,148,475	6,011,246	70,326	137,966	0.521633	0.150037
0.9508	1.0187	4,833,250	6,999,807	70,665	138,025	0.526570	0.150615
1.0447	1.0074	7,273,850	11,309	67,286	137,874	0.499611	0.148170
1.0009	1.0186	5,734,925	4,126,755	69,125	137,960	0.512889	0.149639
0.9939	0.9969	5,507,725	4,920,723	69,971	137,729	0.518166	0.148582
1.0038	0.9837	5,660,250	4,474,926	69,738	137,590	0.516951	0.147694
0.9862	0.9946	5,360,225	5,431,842	70,089	137,692	0.520713	0.148606
0.9811	1.0047	5,334,055	5,445,262	70,158	137,854	0.520160	0.149290
0.9976	1.0129	5,647,625	4,418,700	69,502	137,970	0.514390	0.149377
1.0313	1.0054	7,247,950	10,598	67,899	137,873	0.502476	0.148284
1.0265	0.9998	7,152,350	255,359	68,240	137,803	0.504277	0.148052
1.0360	0.9882	7,217,500	130,558	68,383	137,823	0.503711	0.147359
0.9755	0.9900	5,119,800	6,256,800	70,473	137,709	0.524515	0.148596
0.9778	1.0094	5,289,792	5,589,726	70,207	137,886	0.520600	0.149610
1.0292	0.9912	7,183,800	177,792	68,444	137,753	0.505607	0.147553
0.9597	0.9815	4,856,587	7,292,306	70,905	137,653	0.531141	0.148400
0.9535	0.9830	4,783,162	7,416,720	71,020	137,681	0.533001	0.148590
1.0470	1.0184	7,183,800	177,766	66,820	137,726	0.499780	0.149120
1.0369	1.0124	7,259,625	15,676	67,388	137,847	0.500793	0.148881
1.0093	1.0001	5,835,850	3,854,361	69,476	137,840	0.513070	0.148458
1.0239	0.9838	7,027,475	612,755	68,743	137,522	0.506498	0.147248
1.0495	0.9808	7,275,750	6589	68,196	137,834	0.501815	0.146728
1.0304	1.0186	7,203,275	140,761	67,377	137,820	0.501145	0.149092
1.0384	0.9974	7,254,900	33,762	67,961	137,876	0.502111	0.147722
1.0460	0.9934	7,262,550	19,210	67,838	137,881	0.501235	0.147371
1.0003	0.9908	5,613,700	4,598,846	69,868	137,663	0.516989	0.148123
1.0435	0.9826	7,253,075	15,328	68,302	137,723	0.502930	0.146920
0.9635	1.0142	5,005,907	6,444,320	70,542	137,943	0.524520	0.150200
0.9861	1.0164	5,459,087	5,047,625	69,905	137,918	0.518,270	0.149890
1.0374	0.9812	7,219,825	128,557	68,500	137,641	0.504230	0.146861
1.0113	1.0180	5,940,625	3,439,509	68,654	137,934	0.510464	0.149430
1.0389	1.0186	7,208,815	161,763	67,222	137,808	0.499980	0.149050
1.0495	1.0172	7,228,522	163,151	66,703	137,700	0.499630	0.149090

References

1. Lewis R, Olofsson U (2009) Wheel-rail interface handbook. CRC/Taylor & Francis, Boca Raton
2. Iwnicki S (2006) Handbook of railway vehicle dynamics. CRC/Taylor & Francis, Boca Raton
3. Pombo J, Ambrósio J, Pereira M et al (2011) Development of a wear prediction tool for steel railway wheels using three alternative wear functions. Wear 271(1–2):238–245
4. Wang W, Lewis R, Yang B et al (2016) Wear and damage transitions of wheel and rail materials under various contact conditions. Wear 362–363:146–152
5. Li ZY, Xing XH, Yang MJ et al (2014) Investigation on rolling sliding wear behavior of wheel steel by laser dispersed treatment. Wear 314(1–2):236–240
6. Wang W, Hu J, Guo J et al (2014) Effect of laser cladding on wear and damage behaviors of heavy-haul wheel/rail materials. Wear 311(1–2):130–136
7. Lewis S, Lewis R, Evans G et al (2014) Assessment of railway curve lubricant performance using a twin-disc tester. Wear 314(1–2):205–212
8. Lu X, Cotter J, Eadie D (2005) Laboratory study of the tribological properties of friction modifier thin films for friction control at the wheel/rail interface. Wear 259(7–12):1262–1269
9. Ye Y, Sun Y, Dongfang SP et al (2020) Optimizing wheel profiles and suspensions for railway vehicles operating on specific lines to reduce wheel wear: a case study. Multibody SysDyn. https://doi.org/10.1007/s11044-020-09722-4
10. Fergusson SN, Fröhling RD, Klopper H (2008) Minimising wheel wear by optimising the primary suspension stiffness and centre plate friction of self-steering bogies. Veh Syst Dyn 46(sup1):457–468
11. Mazzola L, Alfi S, Bruni S (2010) A method to optimise stability and wheel wear in railway bogies. Int J Railway 3(3):95–105
12. Bideleh SMM, Berbyuk V, Persson R (2016) Wear/comfort Pareto optimisation of bogie suspension. Veh Syst Dyn 54(8):1053–1076
13. Wan C, Markine V, Shevtsov I (2014) Optimisation of the elastic track properties of turnout crossings. Proc Inst Mech Eng Part F J Rail Rapid Transit 230(2):360–373
14. Pérez J, Busturia J, Goodall R (2002) Control strategies for active steering of bogie-based railway vehicles. Control Eng Pract 10(9):1005–1012
15. Matsumoto A, Sato Y, Ohno H et al (2006) Study on curving performance of railway bogies by using full-scale stand test. Veh Syst Dyn 44(sup1):862–873
16. Fu B, Giossi RL, Persson R et al (2020) Active suspension in railway vehicles: a literature survey. Railway Eng Sci 28(1):3–35
17. Bruni S, Goodall R, Mei TX et al (2007) Control and monitoring for railway vehicle dynamics. Veh Syst Dyn 45(7–8):743–779
18. Wang P, Gao L, Hou BW (2013) Influence of rail cant on wheel-rail contact relationship and dynamic performance in curves for heavy haul railway. Appl Mech Mater 365–366:381–387
19. Gao L, Wang P, Cai X (2018) Superelevation modification for the small-radius curve of Shen-shuo railway under mixed traffic of passenger and freight trains. J Vib Shock 35(18):222–228 **(in Chinese)**
20. Shen G, Ayasse JB, Chollet H et al (2003) A unique design method for wheel profiles by considering the contact angle function. Proc Inst Mech Eng Part F J Rail Rapid Transit 217(1):25–30
21. Shevtsov IY, Markine VL, Esveld C (2003) Optimal design of wheel profile for railway vehicles. In: Proceedings 6th international conference on contact mechanics and wear of rail/wheel systems, Gothenburg, Sweden, pp 231–236
22. Shevtsov IY, Markine VL, Esveld C (2005) Optimal design of wheel profile for railway vehicles. Wear 258(7–8):1022–1030
23. Shevtsov IY, Markine VL, Esveld C (2008) Design of railway wheel profile taking into account rolling contact fatigue and wear. Wear 265(9–10):1273–1282
24. Markine VL, Shevtsov IY (2011) Optimization of a wheel profile accounting for design robustness. Proc Inst Mech Eng Part F J Rail Rapid Transit 225(5):433–442
25. Polach O (2011) Wheel profile design for target conicity and wide tread wear spreading. Wear 271(1–2):195–202
26. Cui D, Li L, Jin X et al (2011) Optimal design of wheel profiles based on weighed wheel/rail gap. Wear 271(1–2):218–226
27. Jahed H, Farshi B, Eshraghi MA et al (2008) A numerical optimization technique for design of wheel profiles. Wear 264(1–2):1–10
28. Sun Y, Zhai W, Ye Y et al (2020) A simplified model for solving wheel-rail non-Hertzian normal contact problem under the influence of yaw angle. Int J Mech Sci 174:105554
29. Sadeghi J, Sadeghi S, Niaki STA (2014) Optimizing a hybrid vendor-managed inventory and transportation problem with fuzzy demand: an improved particle swarm optimization algorithm. Inf Sci 272:126–144
30. Persson I, Iwnicki SD (2004) Optimisation of railway profiles using a genetic algorithm. Veh Syst Dyn 41:517–527
31. Novales M, Orro A, Bugarín MR (2007) Use of a genetic algorithm to optimise wheel profile geometry. Proc Inst Mech Eng Part F J Rail Rapid Transit 221(4):467–476
32. Choi HY, Lee DH, Lee J (2013) Optimisation of a railway wheel profile to minimize flange wear and surface fatigue. Wear 300(1–2):225–233
33. Kennedy J, Eberhart R (1995) Particle swarm optimization, proceedings of IEEE international conference on. Neural Netw. https://doi.org/10.1109/ICNN.1995.488968
34. Lin F, Zhou S, Dong X et al (2019) Design method of LM thin flange wheel profile based on NURBS. Veh Syst Dyn 1(3–4):1–16
35. BS EN 15313 (2016) Railway applications. In-service wheelset operation requirements. In-service and off-vehicle wheelset maintenance
36. Cui DB, Wang RC, Allen P et al (2018) Multi-objective optimization of electric multiple unit wheel profile from wheel flange wear viewpoint. Struct Multidiscip Optim 59:279–289
37. Firlik B, Staśkiewicz T, Jaśkowski W et al (2019) Optimisation of a tram wheel profile using a biologically inspired algorithm. Wear 430–431:12–24
38. Myers RH (2016) Response surface methodology. Wiley, Hoboken
39. Simpson TW, Mauery TM, Korte J et al (2001) Kriging models for global approximation in simulation-based multidisciplinary design optimization. AIAA J 39(12):2233–2241
40. Zakharov S, Goryacheva I, Bogdanov V et al (2008) Problems with wheel and rail profiles selection and optimization. Wear 265(9–10):1266–1272
41. Ignesti M, Innocenti A, Marini L et al (2013) Development of a wear model for the wheel profile optimisation on railway vehicles. Veh Syst Dyn 51(9):1363–1402
42. Molatefi H, Mazraeh A, Shadfar M et al (2019) Advances in Iran railway wheel wear management: a practical approach for selection of wheel profile using numerical methods and comprehensive field tests. Wear 424–425:97–110
43. Spangenberg U, Fröhling RD, Els PS (2018) Long-term wear and rolling contact fatigue behaviour of a conformal wheel profile designed for large radius curves. Veh Syst Dyn 57(1):44–63
44. Santamaria J, Herreros J, Vadillo EG et al (2013) Design of an optimised wheel profile for rail vehicles operating on two-track gauges. Veh Syst Dyn 51(1):54–73

45. Liu B, Mei T, Bruni S (2016) Design and optimisation of wheel–rail profiles for adhesion improvement. Veh Syst Dyn 54(3):429–444
46. UIC Code 518 OR (2009) Testing and approval of railway vehicle from the point of view of their dynamic behavior—safety—track fatigue—running behavior. International Union of Railway
47. BS EN 14363 (2005) Railway applications-testing for the acceptance of running characteristics of railway vehicles-testing of running behavior and stationary tests, CEN, Brussels. https://standards.globalspec.com/std/13162966/en-14363
48. Knothe K, Stichel S (2018) Rail vehicle dynamics. Springer, Berlin
49. Ye Y, Ning J (2019) Small-amplitude hunting diagnosis method for high-speed trains based on the bogie frame's lateral–longitudinal–vertical data fusion, independent mode function reconstruction and linear local tangent space alignment. Proc Inst Mech Eng Part F J Rail Rapid Transit 233(10):1050–1067
50. Wu H (2012) Flange climb derailments: causes and prevention. International Railway Journal. https://www.railjournal.com/in_depth/flange-climb-derailments-causes-and-prevention
51. Schelle H (2014) Radverschleißreduzierung für eine Güterzuglokomotive durch optimierte Spurführung. Technische Universität Berlin, Berlin
52. Reichsbahn D (1965) Strecke Blankenburg—Tanne. Entwurfs- und Vermessungsstelle der Deutschen Reichsbahn, Magdeburg
53. Pfeiffer M, Hecht M (2011) Concept and decision paper: force measurement method for ED-brake-monitoring (electric locomotive—BOMBARDIER TRAXX) incl. data analysis—measurement campaign HVLE, Technische Universität Berlin 2011 (Report No. 11/2011)
54. Ye Y, Shi D, Krause P et al (2019) Wheel flat can cause or exacerbate wheel polygonization. Veh Syst Dyn. https://doi.org/10.1080/00423114.2019.1636098
55. Pearce T, Sherratt N (1991) Prediction of wheel profile wear. Wear 144(1–2):343–351
56. Lewis R, Dwyer-Joyce RS (2004) Wear mechanisms and transitions in railway wheel steels. Proc Inst Mech Eng Part J J Eng Tribol 218(6):467–478
57. Zobory I (1997) Prediction of wheel/rail profile wear. Veh Syst Dyn 28(2–3):221–259
58. EN 13715:2006 + A1:2010 (2011) Railway applications—wheelsets and bogies—Wheels—Tread profile, CEN, Brussels
59. Roshanian J, Ebrahimi M (2013) Latin hypercube sampling applied to reliability-based multidisciplinary design optimization of a launch vehicle. Aerosp Sci Technol 28(1):297–304
60. Ye YG, Shi DC, Krause P et al (2019) A data-driven method for estimating wheel flat length. Veh Syst Dyn. https://doi.org/10.1080/00423114.2019.1620956
61. Hertz H (1982) Über die Berührung fester elastische Körper. Journal für die reine und angewandte Mathematik 1882(92):156–171
62. Sichani MS, Enblom R, Berg M (2016) An alternative to FASTSIM for tangential solution of the wheel–rail contact. Veh Syst Dyn 54(6):748–764
63. Tao GQ, Du X, Wen ZF et al (2017) Development and validation of a model for predicting wheel wear in high-speed trains. J Zhejiang Univ Sci A 18(8):603–616
64. Ye YG, Hecht H (2018) Derailment safety and stability behavior tests of Y25-container wagon with wheel diameter decreasing from 920 mm to 550 mm. Technische Universität Berlin (Report No. 11/2018)
65. Polach O (2006) On non-linear methods of bogie stability assessment using computer simulations. Proc Inst Mech Eng Part F J Rail Rapid Transit 220(1):13–27